Title
Molecular Beam Studies of the Photodissociation of Benzene at 193 and 248 nm

Journal
Journal of chemical physics, 92(71)

Authors
Yokoyama, A.
Zhao, X.
Hintsa, E.J.
et al.

Publication Date
1989-09-01

UC-401
LBL-27736
Preprint

Lawrence Berkeley Laboratory
UNIVERSITY OF CALIFORNIA

Materials & Chemical Sciences Division

Submitted to Journal of Chemical Physics

Molecular Beam Studies of the Photodissociation of Benzene at 193 and 248 nm

A. Yokoyama, X. Zhao, E.J. Hintsa, R.E. Continetti, and Y.T. Lee

September 1989

Prepared for the U.S. Department of Energy under Contract Number DE-AC03-76SF00098.

DISCLAIMER

Molecular Beam Studies of the Photodissociation of Benzene at 193 and 248 nm

A. Yokoyama,* X. Zhao, E. J. Hintsa, R. E. Continetti, and Y. T. Lee

Materials and Chemical Sciences Division, Lawrence Berkeley Laboratory and Department of Chemistry, University of California, Berkeley, California 94720

ABSTRACT

The photodissociation processes of benzene following excitation at 193 and 248 nm have been studied by molecular beam photofragmentation translational spectroscopy. When benzene was excited to the $^1B_{1u}$ state by absorption at 193 nm, dissociation occurred through three primary channels, $C_6H_5 + H$ (80%), $C_6H_4 + H_2$ (16%), and $C_5H_3 + CH_3$ (4%), following internal conversion to the vibrationally excited ground state. When benzene was excited to the $^1B_{2u}$ state at 248 nm, two primary dissociation channels, $C_6H_4 + H_2$ (96%), and $C_5H_3 + CH_3$ (4%), were observed. Photodissociation to produce two C_3H_3 was induced by two photon absorption of benzene at both 193 and 248 nm. Numerous secondary photodissociation processes of the primary photoproducts were also observed at both 193 and 248 nm.

I. INTRODUCTION

Although there has been extensive study of the photophysics and photochemistry of benzene,[1,2] its primary photodissociation processes are still poorly understood. In the photolysis of benzene at 184.9 nm,[3,4] the quantum yield for the disappearance of benzene was found to decrease from unity at the low pressure limit with increasing benzene or N_2 buffer gas pressures. The main photoproducts were reported to be an isomer of benzene, subsequently identified as fulvene,[5,6] and polymers. Cis- and trans-1,3-Hexadien-5-yne were also identified as photoproducts,[7,8] and small amounts of other compounds, i.e. methane, ethane, ethylene, hydrogen and acetylene, were observed as well.[3,9] The quantum yields of fulvene and 1,3-hexadien-5-yne fell off at high and low N_2 pressures, and extrapolated to zero at zero pressure.[8]

From the pressure dependence of the quantum yields for the disappearance of benzene and the production of benzene isomers, a reaction mechanism proceeding through the vibrationally excited ground electronic state of benzene, "hot benzene", was proposed.[4,8] Hot benzene is produced through internal conversion (IC) from the electronically excited singlet state ($^1E_{1u}$ or $^1B_{1u}$) populated by 184.9 nm absorption, and has also been observed after 193 nm excitation to the $^1B_{1u}$ state.[10] Various vibrationally hot isomers can be produced from hot benzene in competition with collisional deexcitation. The vibrationally

hot isomers are then collisionally stabilized or else react to form dissociation products and polymers.

When benzene in the gas phase is excited to the lowest excited singlet state ($^1B_{2u}$), the excited benzene molecules relax through IC,[11] intersystem crossing,[12] fluorescence,[12] and isomerization to benzvalene,[12,13] with no evidence of any dissociation. However, new photodissociation channels could open up under collision-free conditions, because the possibility of collisional relaxation of hot molecules is removed and energy loss through infrared emission from hot benzene is comparatively slow.

There have been many studies[14,15] of the UV photodissociation of benzene under collision-free conditions, but the observed species have been limited to ions resulting from multiphoton ionization (MPI)/fragmentation processes, and there has been no report of the primary photodissociation processes resulting in neutral fragments under these conditions. Molecular beam photofragmentation translational spectroscopy can be used to elucidate the neutral reaction pathways in photodissociation and has been successfully applied in a series of studies of the concerted decomposition of cyclic organic molecules.[16-18] In this work, a study of the photodissociation channels of benzene at 193 and 248 nm is presented.

II. EXPERIMENTAL

Two types of molecular beam apparatus were used in this investigation. A rotating source machine (RSM) used for most of this study has been described in detail elsewhere.[19] The benzene beam was produced by expanding a benzene/Ar or benzene/He mixture at about 100 torr into the source chamber through a .125 mm nozzle. The nozzle was heated to 110-130 °C to prevent the formation of benzene clusters. The benzene/rare gas mixture was prepared by bubbling Ar or He through benzene at 5 °C, where it has an equilibrium vapor pressure of about 30 torr. The molecular beam was collimated by passing through two skimmers in differential pumping regions. The peak velocities of the beam were typically 6.35×10^4 and 8.00×10^4 cm/s with a FWHM of about 20% for the benzene/Ar and benzene/He mixtures, respectively. The benzene beam was crossed perpendicularly with a laser beam focused to a 6×2 mm^2 spot at the crossing point 10 cm from the nozzle with a MgF_2 lens. Dissociation products of benzene at 193 and 248 nm were detected at beam-to-detector angles of 8° to 15°. A Lambda-Physik EMG 103 MSC excimer laser was used as the light source and operated at 100 Hz with ArF (193 nm) or KrF (248 nm) gas mixtures. The laser power was monitored after passing through the interaction region.

For the detection of H and H_2 fragments at 193 nm, a crossed molecular beam apparatus (CMBA) with a rotatable mass spectrometer detector, described in ref. 20, was used. This

apparatus has been specially configured to produce fast H atoms by photolysis for reactive scattering experiments, and is ideal for studying H and H_2 production by photodissociation in the beam source. Deuterated benzene (C_6D_6) was used to study D_2 elimination, as it was difficult to obtain high quality data for H_2 at mass-to-charge ration (m/e) = 2 due to the large inherent partial pressure of H_2 in the mass spectrometer. For all the experiments carried out on the CMBA, a neat benzene beam was produced by expanding benzene through a pulsed valve with a nozzle diameter of 1 mm and collimating it with a 1.5 mm diameter skimmer. Stagnation pressures of benzene behind the valve ranged from 20 to 40 torr. The benzene beam was crossed perpendicularly with the laser beam which was focused to 3×3 mm at the crossing point 3 cm from the nozzle. Fragments were observed at an angle perpendicular to both beams.

III. RESULTS AND ANALYSIS

A. 193 nm

Photodissociation signal from benzene was observed at m/e = 12-15, 24-27, 36-39, 48-51, 60-62, and 72-77 with the RSM, and at m/e = 1 and 2 with the CMBA. The time-of-flight (TOF) spectrum obtained at m/e = 77 ($C_6H_5^+$) is shown in Fig. 1(a). This signal must come from phenyl radical (C_6H_5) produced by the reaction:

$$C_6H_6 \xrightarrow{h\nu} C_6H_5 + H \qquad (1)$$

The solid line represents the calculated TOF spectrum using the translational energy distribution ($P(E_T)$) for reaction (1), shown in Fig. 2. The $P(E_T)$ was determined by forward convolution methods[19] and was obtained here by simultaneously fitting the m/e = 77 TOF spectra at 10° and 15° and the m/e = 1 spectrum at 90°, shown in Fig. 1(b). The high energy tail in Fig. 2 extending out to 39 kcal/mol is necessary to fit the m/e = 77 spectrum at 15°. Since only C_6H_5 with more than 6 kcal/mol of translational energy can reach the detector at 10°, the $P(E_T)$ for reaction (1) at lower translational energies was determined only from the m/e = 1 spectrum. H atoms from secondary dissociation (reaction (3a) below) also contribute to the m/e = 1 spectrum, and this secondary reaction was arbitrarily assumed to have the same $P(E_T)$ as that for reaction (1).

The TOF spectrum at m/e = 76 ($C_6H_4^+$), shown in Fig. 3(a), contains a new component at shorter arrival times than the

daughter ion peak of C_6H_5. This is attributed to benzyne (C_6H_4) produced by H_2 elimination:

$$C_6H_6 \xrightarrow{h\nu} C_6H_4 + H_2 \qquad (2)$$

The $P(E_T)$ for this reaction is shown in Fig. 4(a). The m/e = 2 TOF spectrum showed that the fastest H_2 velocity is faster than that predicted by the $P(E_T)$ derived from the m/e = 76 data. Since the laser intensity in the CMBA experiment was about ten times higher than in the RSM experiment, secondary photodissociation of primary photoproducts is more important and the broader velocity spread of the H_2 formed in secondary photodissociation processes partially obscures the primary dissociation signal. Some of the observed H_2 may also come from MPI/fragmentation processes such as those observed in ref. 14. The TOF spectra at m/e = 72-75 (C_6^+ - $C_6H_3^+$) show only one peak, similar to those at m/e = 76 and 77. However, the peak shifts to shorter flight times and becomes broader with decreasing m/e. This is due to secondary photodissociation of the primary photoproducts through reactions (3a) and (3b).

$$C_6H_5 \xrightarrow{h\nu} C_6H_4 + H \qquad (3a)$$

$$C_6H_4 \xrightarrow{h\nu} C_6H_3 + H \qquad (3b)$$

A laser power dependence study of the m/e = 75 TOF spectrum shows that the peak shifts to longer flight times and becomes narrower with decreasing laser power as shown in Fig. 3(b). At the lowest laser power used, the shape is almost the same as that at m/e = 76.

The TOF spectra at m/e = 60-62 contain two peaks as shown in Fig. 5(a). The slow component is from reactions (1) and (2) while the faster component is due to a fragment containing five carbon atoms, which could be from either C_5H_2 + CH_4 or C_5H_3 + CH_3. Of the corresponding one carbon fragments, only CH_3^+ or lighter ions were observed. If CH_4 were produced, signal at m/e = 16 (CH_4^+) should be detected, because CH_4 is very stable and CH_4^+ is the most abundant ion in the mass spectrum of CH_4. On the other hand, $C_5H_3^+$ may be only weakly bound and vibrationally excited C_5H_3 may produce only $C_5H_2^+$ or smaller ions in the ionizer. Therefore, the fragment detected at m/e = 15 containing one carbon atom is methyl radical (CH_3) and the fast component appearing in the m/e = 62 TOF spectrum from the reaction:

$$C_6H_6 \xrightarrow{h\nu} C_5H_3 + CH_3 \qquad (4)$$

The $P(E_T)$ for this reaction, shown in Fig. 6(a), was obtained by fitting the m/e = 60-62 TOF spectra. On the CMBA, both m/e 15 (CH_3^+) from C_6H_6 and m/e 18 (CD_3^+) from C_6D_6 photolysis were observable. Due to circumstances beyond our control, a complete m/e 15 spectrum was not recorded. The fit to the m/e 18 (CD_3^+) data, shown in Fig. 5(a), is consistent with rxn. (4). This spectrum was fit by assuming that the $P(E_T)$ for the photodissociation of C_6D_6 to CD_3 and C_5D_3 was the same as that for reaction (4). The result is the solid curve in figure 5(b). The agreement between the calculated and observed fast edges of the TOF spectra supports the conclusion that part of

the signal at m/e = 15 (m/e = 18 for C_6D_6) comes from CH_3 (CD_3) produced by reaction (4).

The m/e = 51 TOF spectrum contains a new component which is faster than the daughter ions of fragments produced by reactions (1-4), as shown in Fig. 7(a). This peak is also observed in the m/e = 48-50 TOF spectra. A fast component in the m/e = 24-27 TOF spectra matches this component by conservation of linear momentum as shown in Fig. 7(b), assuming a reaction producing fragments with two and four carbon atoms. The heaviest ions detected were m/e = 51 ($C_4H_3^+$) for the fragment containing four carbon atoms, as shown in Table 1, and m/e = 27 ($C_2H_3^+$) for the two carbon fragment. Therefore, the following reaction is an obvious choice to explain these components:

$$C_6H_6 \xrightarrow{h\nu} C_4H_3 + C_2H_3 \qquad (5)$$

The intensity ratio of m/e = 27 to m/e = 26 signal from C_2H_3 produced in the photodissociation of C_2H_3Br at 193 nm was measured to be ca. 5.[21] Therefore, the intensity at m/e = 27 here should be larger than that at m/e = 26, if reaction (5) were the dominant channel. However, since the measured intensity ratio was only 0.08, the contribution of reaction (5) is not significant and the fast component in the TOF spectra at m/e = 24-26 must come from C_2H_2. The following dissociation reaction of phenyl radical has been proposed as a result of pyrolysis studies of benzene:[22]

$$C_6H_5(\text{phenyl}) \longrightarrow C_6H_5(\text{linear}) \longrightarrow C_4H_3 + C_2H_2 \qquad (6)$$

For this reaction to occur, the phenyl radical must absorb another photon. A power dependence study of the fast components in the TOF spectra at m/e = 26 and 51 showed that they are in fact produced by two photon absorption. Another candidate for the reaction producing these components is the direct dissociation of benzene to C_2H_2 and C_4H_4:

$$C_6H_6 \xrightarrow{h\nu} C_4H_4 + C_2H_2 \qquad (7)$$

Although signal at m/e = 52 ($C_4H_4^+$) was not observed, there exist cases where the parent ion of a photofragment is not observed, because the fragment is internally excited and dissociates after ionization.[23] From a simulation of the TOF spectra we could not determine which channel is predominant, but according to a rate equation model for the power dependence of fragment yields (see discussion), reaction (6) best explains the origin of the fast components appearing in the TOF spectra at m/e = 24-27 and 48-51. The $P(E_T)$ for reaction (6) is shown in Fig. 8(a). Although the photodissociation of C_6H_4, which was observed at 248 nm as described later, may also produce C_2H_2 and C_4H_2, no evidence for this reaction was observed in the TOF spectra at 193 nm. This may be partly due to the fact that at 193 nm C_6H_5 production is more important than C_6H_4 production.

The fast component appearing in the m/e = 36-39 TOF spectra, shown in Fig. 9, indicates yet another dissociation

channel. This channel is ascribed to the following reaction:

$$C_6H_6 \xrightarrow{2h\nu} 2C_3H_3 \qquad (8)$$

The $P(E_T)$ obtained for this reaction is shown in Fig. 10(a).

(B) 248 nm

Since the heaviest ion detected was $C_6H_4^+$, H atom elimination does not occur at 248 nm. Because the photon energy (115 kcal/mol) is only slightly larger than the endothermicity of reaction (1) (110.8 kcal/mol),[24] the C-H bond rupture rate in the ground electronic state is expected to be much slower than that of other reactions described below. The m/e = 76 ($C_6H_4^+$) TOF spectrum, shown in Fig. 11(a), indicates the occurrence of reaction (2). The $P(E_T)$ for this reaction is shown in Fig. 4(b). Although the shape of the TOF spectrum at m/e = 75 is the same as that at m/e = 76, another component appears at the fast edge of the m/e = 72-74 TOF spectra. As shown in Fig. 11(b), the relative contribution of this component decreases with decreasing laser power, and the shape is almost the same as that at m/e = 76 at the lowest laser power used. Therefore, this component is likely to be from the following reaction:

$$C_6H_4 \xrightarrow{h\nu} C_6H_2 + H_2 \qquad (9)$$

The $P(E_T)$ for this reaction is shown in Fig. 12. A fast component due to reaction (4) (loss of CH_3) appears in the TOF spectra at m/e = 60-62 as shown in Fig. 13. The $P(E_T)$ for this reaction at 248 nm is shown in Fig. 6(b).

The fast component in the m/e = 48-51 TOF spectra, an example of which is shown in Fig. 14, also indicates the presence of dissociation to fragments containing two and four carbon atoms. However, the intensity at m/e = 51 here is very low compared with that at m/e = 50, as shown in Table 1 along with the corresponding intensities measured at 193 nm. This indicates that the dissociation may be as follows:

$$C_6H_4 \xrightarrow{h\nu} C_4H_2 + C_2H_2 \qquad (10)$$

This is reasonable, since no C_6H_5 formation is observed at 248 nm. The $P(E_T)$ for this reaction is shown in Fig. 8(b). Both the maximum and average translational energy release of this reaction are larger than those for reaction (6). On the other hand, the maximum and average energies of the $P(E_T)$'s for the other reaction channels at 248 nm are smaller than those for the same channels at 193 nm. This also supports the argument that the dissociation channel leading to fragments containing two and four carbon atoms is different between 193 and 248 nm, and is not the direct photodissociation of benzene (reaction (7)) but photodissociation of photoproducts (reactions (6) and (10)).

The TOF spectrum at m/e = 39 ($C_3H_3^+$) is shown in Fig. 15. Since daughter ions from reaction (10) cannot appear in this spectrum, the fast component must come mainly from reaction (8). Fig. 10(b) shows the $P(E_T)$ for this reaction obtained by fitting the TOF spectrum.

All the dissociation channels observed at both 193 and 248 nm with their translational energy releases are listed in Table 2. The benzene molecules in a molecular beam, produced from a nozzle at 100-130°C, are expected to contain substantial amount of internal energies. The average excitation energy after photoexcitation can be as much as 6-8 kcal/mole beyond the photon energy.

IV. DISCUSSION

(A) Dissociation mechanism at 193 nm

Benzene molecules in the ground state (S_0) are excited to the $^1B_{1u}$ state (S_2) by absorption at 193 nm. Reilly and Kompa[14] observed multiphoton ionization of benzene through the S_2 state using an ArF laser. They determined the lifetime of S_2 to be 20 ps by comparing the power dependence of the total ion yield with the theoretical curve derived using a rate equation containing S_0, S_2 and the ground state of benzene ion (B^+). In their model, the absorption cross-section of S_2 at 193 nm (leading to ionization) was assumed to be 7.5×10^{-17} cm^2, independent of the identity of the lower state. Using this value, the transition rate between S_2 and B^+ can be calculated to be only 2×10^9 s^{-1} even at the highest laser intensity of 27 MW/cm^2 in this experiment. This implies that the relaxation rate ($1/\tau$) of S_2 is more than 25 times higher than the transition rate between S_2 and B^+, and most of the molecules in S_2 relax to lower electronic states. Furthermore, Nakashima and Yoshihara[10] have observed transient spectra of "hot benzene" (S_0^*), after excitation to S_2 with an ArF laser. Therefore, the observed photochemical reactions occur after the production of hot benzene by IC from S_2 to S_0^*. In fact, the observed $P(E_T)$'s for simple bond rupture peak at zero kinetic energy release, typical for such reactions on the ground electronic potential energy surface with no exit barrier.[23]

In the analysis of our experiments, a rate equation model based on the seven-level system depicted in Fig. 16 is used to interpret the power dependence of the fragment yields. In Fig. 16, P_1 represents a fragment produced by the dissociation of hot benzene (one photon process), P_2 a fragment produced after hot benzene absorbs one more photon (two photon process), and P_3 a fragment produced after photoabsorption by the product P_1 (secondary photodissociation). The rate equations are written as follows:

$$d[S_2]/dt = \sigma_1 I[S_0] - (\sigma_2 I + \sigma_3 I + 1/\tau)[S_2]$$

$$d[B^+]/dt = \sigma_3 I[S_2]$$

$$d[S_0^*]/dt = 1/\tau[S_2] - (\sigma_4 I + k)[S_0^*]$$

$$d[P_1]/dt = k[S_0^*] - \sigma_5 I[P_1]$$

$$d[P_2]/dt = \sigma_4 I[S_0^*]$$

$$d[P_3]/dt = \sigma_5 I[P_1]$$

with the constraint of conservation of mass;

$$[S_0]_0 = [S_0] + [S_2] + [B^+] + [S_0^*] + [P_1] + [P_2] + [P_3]$$

where the σ's are the photo-absorption cross-sections, τ is the lifetime of the S_2 state, k is the dissociation rate constant from S_0^*, $[S_0]_0$ is the initial concentration of S_0, and I is the laser intensity in units of photons/cm^2. The dissociation rates for the precursor states to P_2 and P_3 are assumed to be fast compared with the photoabsorption rates of S_0^* and P_1. The above rate equations can be solved by assuming that the laser intensity is homogeneous and has a rectangular temporal profile. If laser irradiation starts at t = 0, the concentra-

tions of each state at the end of the laser pulse, t = T, are as follows:

$$[S_2] = \frac{\sigma_1 I[S_0]_0}{\lambda_1 - \lambda_2} (e^{\lambda_1 T} - e^{\lambda_2 T})$$

$$[S_0^*] = \frac{1/\tau\sigma_1 I[S_0]_0}{\lambda_1 - \lambda_2} \{ \frac{(\lambda_1 - \lambda_2)e^{-\mu T}}{(\lambda_2 + \mu)(\lambda_1 + \mu)} + \frac{e^{\lambda_1 T}}{\lambda_1 + \mu} - \frac{e^{\lambda_2 T}}{\lambda_2 + \mu} \}$$

$$[P_1] = \frac{1/\tau k\sigma_1 I[S_0]_0}{\lambda_1 - \lambda_2} \{ \frac{(\lambda_1 - \lambda_2)e^{-\mu T}}{(\lambda_2 + \mu)(\lambda_1 + \mu)(\sigma_5 I - \mu)}$$

$$- \frac{(\lambda_1 - \lambda_2)e^{-\sigma_5 IT}}{(\lambda_2 + \sigma_5 I)(\lambda_1 + \sigma_5 I)(\sigma_5 I - \mu)} + \frac{e^{\lambda_1 T}}{(\lambda_1 + \sigma_5 I)(\lambda_1 + \mu)}$$

$$- \frac{e^{\lambda_2 T}}{(\lambda_2 + \sigma_5 I)(\lambda_2 + \mu)} \}$$

$$[P_2] = \frac{1/\tau\sigma_1\sigma_4 I^2[S_0]_0}{\lambda_1 - \lambda_2} \{ \frac{e^{\lambda_1 T}}{\lambda_1(\lambda_1 + \mu)} - \frac{e^{\lambda_2 T}}{\lambda_2(\lambda_2 + \mu)}$$

$$- \frac{(\lambda_1 - \lambda_2)e^{-\mu T}}{\mu(\lambda_1 + \mu)(\lambda_2 + \mu)} + \frac{\lambda_1 - \lambda_2}{\lambda_1\lambda_2\mu} \}$$

$$[P_3] = \frac{1/\tau k\sigma_1\sigma_5 I^2[S_0]_0}{\lambda_1 - \lambda_2} \{ \frac{e^{\lambda_1 T}}{\lambda_1(\lambda_1 + \mu)(\lambda_1 + \sigma_5 I)}$$

$$- \frac{e^{\lambda_2 T}}{\lambda_2(\lambda_2 + \sigma_5 I)(\lambda_2 + \mu)} - \frac{(\lambda_1 - \lambda_2)e^{-\mu T}}{\mu(\lambda_2 + \mu)(\lambda_1 + \mu)(\sigma_5 I - \mu)}$$

$$+ \frac{(\lambda_1 - \lambda_2)e^{-\sigma_5 IT}}{\sigma_5 I(\lambda_2 + \sigma_5 I)(\lambda_1 + \sigma_5 I)(\sigma_5 I - \mu)} + \frac{\lambda_1 - \lambda_2}{\sigma_5 I \lambda_1 \lambda_2 \mu}\}$$

where

$$\lambda_{1,2} = \frac{-\theta_1 \pm \sqrt{\theta_1^2 - 4\theta_2}}{2}$$

$$\theta_1 = (\sigma_1 + \sigma_2 + \sigma_3)I + 1/\tau$$

$$\theta_2 = \sigma_1 I(\sigma_3 I + 1/\tau)$$

$$\mu = \sigma_4 I + k$$

Product yields for one photon processes are proportional to the sum of $[S_2]$, $[S_0^*]$ and $[P_1]$, because molecules in S_2 and S_0^* at the end of the laser pulse will eventually dissociate and produce P_1. Product yields for two photon dissociation and secondary photodissociation are proportional to $[P_2]$ and $[P_3]$, respectively.

The ground state absorption cross-section (σ_1) is 8.3×10^{-18} cm^2 at 193 nm.[14] The stimulated emission cross-section for the same transition (σ_2) is assumed to be equal to σ_1. The absorption cross-section of S_2 (σ_3) and the lifetime τ of S_2 are also known to be 7.5×10^{-17} cm^2 and 20 ps,[14] respectively. The absorption cross-section of S_0^* (σ_4) is 1.5×10^{-17} cm^2 at 193 nm, which is the extrapolated value from the measured wavelength dependence of the absorption cross-section of hot benzene using the Sulzer-Wieland model.[10] Since we do not know the dissociation rate constant k, we calculated the power dependence of the yields using several values of k ranging from

3×10^5 to 1×10^8 s^{-1}. The photoproduct absorption cross-section σ_5 was determined by fitting the theoretical curves to the data. Since the absolute yields were not determined, $[S_0]_0$ was used as a fitting parameter.

Figs. 17(a) and (b) show the power dependence of the C_5H_3 and C_3H_3 yields produced in reactions (4) and (8), respectively. The lines in these figures show the calculated power dependence for various values of k. The C_5H_3 yield was fit to the power dependence curve for one photon processes ($[S_2]$ + $[S_0^*]$ + $[P_1]$) with $\sigma_5 = 0$. Both the experimental data and calculated curves show strong saturation, and better agreement is obtained at higher k. The agreement between the experimental and calculated results indicates that reaction (4) occurs through a one photon process and the secondary photodissociation of C_5H_3 products is not important. A two photon power dependence curve ($[P_2]$) fit the yield of C_3H_3 well, indicating that reaction (8) occurs through a two photon process. The ratio of the product yield for two photon processes to that for one photon processes was calculated to be 0.6 with $k = 5 \times 10^7$ s^{-1} at a laser intensity of 5 MW/cm^2, while the measured ratio was about 0.2. Although the calculated ratio is 3 times higher than the measured one, this may be partly due to the uncertainty in the cross-sections used and to the assumed temporal profile of the laser pulse.

Fig. 17(c) shows the power dependence of the fast components of the TOF spectra at m/e = 25 and 48, which were ascribed

to reactions (6) or (7). The dashed line drawn in this figure shows the calculated power dependence for the two photon process ($[P_2]$) which corresponds to reaction (7). The agreement between the calculated and experimental results is poor. Therefore, the experimental data were fit to the power dependence curve for secondary photodissociation ($[P_3]$) which corresponds to reaction (6). Since we do not know the absorption cross-section σ_5 of C_6H_5, it was used as a fitting parameter together with $[S_0]_0$. The solid line shows the result with $k = 5 \times 10^7\ s^{-1}$. σ_5 ranges from $5.2 \times 10^{-17}\ cm^2$ to $5.5 \times 10^{-17}\ cm^2$, depending on the value of k used. The fragment yield ratio for secondary photodissociation compared to one photon processes at a laser intensity of 5 MW/cm^2 was calculated to be 2×10^{-3} and 0.3 for $k = 3 \times 10^5\ s^{-1}$ and $5 \times 10^7\ s^{-1}$, respectively. The exact value is difficult to determine from the experimental data, because the TOF spectra are composed of fragments from many reaction channels. However, the measured ratio is estimated to be about 0.8. Therefore, it is concluded that k should be at least on the order of $10^7\ s^{-1}$ to explain the experimental results.

Fig. 17(d) shows the power dependence of C_6H_5 and C_6H_4 produced in reactions (1) and (3a), respectively. Fig. 17(e) shows the power dependence of C_6H_4 and C_6H_3 produced by reactions (2) and (3b). The solid and broken lines in these figures indicate the calculated power dependence for the one photon processes ($[S_2] + [S_0^*] + [P_1]$) and for secondary

photodissociation ([P_3]), respectively. The value of σ_5 determined from the power dependence of C_4H_3 and C_2H_2 was used for this calculation. The agreement between the experimental and calculated results for the one photon process is not perfect. However, the effects of saturation are well reproduced by the calculated curves.

From an analysis of the power dependences with the rate equation model, it is concluded that the following dissociation mechanism as shown in Fig. 18 best describes the photodissociation processes of benzene at 193 nm. Most of the benzene excited to S_2 relaxes to S_0 through IC, producing hot benzene molecules. The hot benzene spontaneously dissociates to C_6H_5 + H, C_6H_4 + H_2 and C_5H_3 + CH_3. Absorption of a second photon by hot benzene results in dissociation to produce two C_3H_3. Absorption by C_6H_5 results in dissociation to C_4H_3 + C_2H_2 and C_6H_4 + H. Photodissociation of C_6H_4 to C_6H_3 + H also occurs following absorption by C_6H_4. Using methods described in ref. 16, the relative primary product yields were obtained to be 0.8 for reaction (1), 0.16 for reaction (2) and 0.04 for reaction (4).

(B) Dissociation mechanism at 248 nm

S_0 benzene is excited to the $^1B_{2u}$ state (S_1) by absorption at 248 nm. Reilly and Kompa[14] used 3.4×10^{-17} cm^2 for the absorption cross-section of S_1 (σ_3) at 248 nm in their rate equation model of the power dependence of the total ion yield

from the multiphoton ionization of benzene. If we use this value, the absorption rate in S_1 is 24 times higher than the relaxation rate to S_0^*, which is the reciprocal of the S_1 lifetime (τ = 28 ns),[25] at a laser intensity of 20 MW/cm^2. Therefore, most molecules in S_1 should have ionized under our experimental conditions and the power dependences of all the fragment yields should have shown strong saturation effects, even the two photon processes. However, as shown in Fig. 18, the experimental power dependences did not show strong saturation and the high signal level from neutral dissociation products also suggests that ionization from S_2 is not the dominant process. Nakashima et al.[11,26] observed the transient absorption spectrum of benzene after 248 nm excitation. They assigned a peak at 270 nm as the transition from S_1 to the 2^1E_{2g} state, with a molar extinction coefficient of 1900 $M^{-1}cm^{-1}$ at 255.4 nm. Therefore, we estimate the absorption cross-section of S_1 to be 2.6×10^{-18} cm^2 at 248.4 nm from the absorption spectrum in ref. 26. This value is about an order of magnitude less than that used in ref. 14 and seems to be more reasonable in explaining the power dependence results.

At 248 nm, the processes are somewhat simpler, and a rate equation model based on a five-level system was used to interpret the power dependence of the fragment yields at 248 nm. In this model, the S_1 state connects directly to P_1 by spontaneous dissociation with a rate of $1/\tau$ and to P_2 by absorption of a second photon. Although the P_1 state, which

corresponds to one photon processes, is connected directly to S_1, this does not necessarily imply direct dissociation on an electronically excited potential energy surface correlating to S_1. If the molecules in S_1 relax to a lower triplet state or to S_0^* and then dissociate to form products with one rate determining step controlling the process, the same model could explain our power dependence results. An appreciable amount of secondary photoproducts were observed as will be described later, so substantial dissociation of primary products must be occurring within the laser pulse duration (16 ns). Since reactions (2) and (4) release a low average amount of kinetic energy, S_0^* is most likely the intermediate in these reactions. The concentration of each state at the end of the laser pulse can be obtained as the following relations in a similar way to the analysis at 193 nm.

$$[S_1] = \frac{\sigma_1 I [S_0]_0}{\lambda_1 - \lambda_2} (e^{\lambda_1 T} - e^{\lambda_2 T})$$

$$[P_1] = \frac{1/\tau\sigma_1 I [S_0]_0}{\lambda_1 - \lambda_2} \{\frac{(\lambda_1 - \lambda_2) e^{-\sigma_4 I T}}{(\lambda_1 + \sigma_4 I)(\lambda_2 + \sigma_4 I)} + \frac{e^{\lambda_1 T}}{\lambda_1 + \sigma_4 I} - \frac{e^{\lambda_2 T}}{\lambda_2 + \sigma_4 I}\}$$

$$[P_2] = \frac{\sigma_1 \sigma_3 I^2 [S_0]_0}{\lambda_1 - \lambda_2} \{\frac{e^{\lambda_1 T}}{\lambda_1} - \frac{e^{\lambda_2 T}}{\lambda_2} + \frac{\lambda_1 - \lambda_2}{\lambda_1 \lambda_2}\}$$

$$[P_3] = \frac{1/\tau\sigma_1\sigma_4 I^2 [S_0]_0}{\lambda_1 - \lambda_2} \left\{ \frac{e^{\lambda_1 T}}{\lambda_1(\lambda_1 + \sigma_4 I)} - \frac{e^{\lambda_2 T}}{\lambda_2(\lambda_2 + \sigma_4 I)} \right.$$

$$\left. - \frac{(\lambda_1 - \lambda_2)e^{-\sigma_4 IT}}{\sigma_4 I(\lambda_1 + \sigma_4 I)(\lambda_2 + \sigma_4 I)} + \frac{\lambda_1 - \lambda_2}{\lambda_1\lambda_2\sigma_4 I} \right\}$$

where σ_4 is the absorption cross-section of P_1.

The ground state absorption cross-section (σ_1) is 1.4×10^{-19} cm^2 at 248 nm.[11] The stimulated emission cross-section for the same transition (σ_2) is assumed to be equal to σ_1. The absorption cross-section of S_1 (σ_3) and lifetime τ of S_1 are 2.6×10^{-18} cm^2 and 28 ns, respectively.[25,26] Since we do not know the absorption cross-section σ_4 of the products, we calculated the power dependence curve at several different values ranging from 2×10^{-21} to 1×10^{-16} cm^2. Fig. 18(a) shows the power dependence of the C_5H_3 yield produced by reaction (4). The experimental data are fit well by the calculated power dependence curve for one photon processes ($[S_1] + [P_1]$) with $\sigma_4 = 0$, drawn as the solid line in this figure. $\sigma_4 = 0$ again indicates that the photodissociation of C_5H_3 product is not occurring. The power dependence of C_3H_3 produced by reaction (8) was fit to the calculated power dependence for two photon processes ($[P_2]$) as shown in Fig. 18(b). The calculated ratio of the product yields for two photon to one photon processes is 0.8 with $\sigma_4 = 5 \times 10^{-17}$ cm^2 at a laser intensity of 25 MW/cm^2, in good agreement with the observed ratio of approximately 0.7. Fig. 18(c) shows the

power dependence of C_4H_2 produced by reaction (10). The line indicates the calculated signal from secondary photodissociation ($[P_3]$). Although the calculated curve changes little with changing σ_4, the fraction of products from secondary photodissociation compared to the initial benzene concentration depends strongly on it. The ratio of fragment yield for secondary photodissociation to that for one photon processes at a laser intensity of 25 MW/cm^2 was calculated to be 5×10^{-4} and 0.4 at σ_4 values of 1×10^{-20} and 5×10^{-17} cm^2, respectively. This ratio does not change for σ_4 larger than 5×10^{-17} cm^2, because all primary products produced within the laser pulse should absorb another photon and dissociate. On the other hand, the observed ratio was about 2 at the same laser intensity. Although the agreement between the calculated and measured ratios is not very good, σ_4 is probably on the order of 10^{-17} cm^2. Fig. 18(d) shows the power dependence of C_6H_4 and C_6H_2 produced by reactions (2) and (9), respectively. The C_6H_4 and C_6H_2 yields were fit to the calculated curves for one photon and secondary photodissociation processes, respectively. Since the fits shown in the figure are reasonably good, reaction (2) should be due to one photon absorption.

The relative amounts of the primary dissociation channels were obtained to be 0.96 for reaction (2) and 0.04 for reaction (4). The important dissociation processes involved are shown in Fig. 20.

(C) Multiphoton ionization/fragmentation processes

The mechanism for the extensively investigated MPI/fragmentation processes of benzene is believed to be MPI followed by the dissociation of benzene ion by successive photoabsorption.[27] When comparing fragment ions observed in MPI studies[15] and neutral fragments observed in this study, there are many species such as C_5H_3, C_4H_3, C_3H_3 and C_2H_2 which appear both as fragment ions and as neutral products. Therefore, some of the fragment ions are very likely produced by photoionization of neutral fragments. This ionization process may be especially important at 193 nm, where most of the benzene molecules in S_2 relax to S_0 even at a laser intensity of 27 MW/cm^2, as described above.

(D) Energetics of the C_5H_3 + CH_3 channel and structure of C_5H_3

Of the primary channels, dissociation to C_5H_3 and CH_3 is the most surprising, because H atoms must migrate until one carbon atom gathers three H atoms and the C-C bond breaks. Considering the energetics of C-C bond rupture, excitation at 248 nm, which deposits 115 kcal/mol of energy in the molecule, is insufficient to break apart the benzene ring. However, at this level of excitation, H-migration and isomerization must be facile, and in retrospect it is quite understandable that only the formation of an isomer containing a C-C single bond, i.e. C_5H_3-CH_3, will lead to C-C bond rupture. Accumulation of three H atoms on a terminal carbon is the key to C-C bond rupture and

CH_3 formation. Neutral CH_3 fragments have also been observed in the electron impact ionization of benzene.[28]

The energy available for this reaction, which is calculated by subtracting the observed maximum translational energy release from the photon energy, is estimated to be 114 and 85 kcal/mol at 193 and 248 nm, respectively, as shown in Table 2. The heats of formation of several benzene isomers having a CH_3 group were calculated by the group additivity method of Benson[24] and listed in Table 3. Since there is no reported value for the ring correction for 5-methyl-1-cyclopentene-3-yne, we used that of 1,3-cyclopentadiene. The heats of formation for all the linear molecules are larger than 93 kcal/mol. If we add typical C-C bond dissociation energies of 80-90 kcal/mol to the heat of formation of the linear molecules and subtract the heat of formation for benzene (19.8 kcal/mol), the heat of reaction for the dissociation to C_5H_3 and CH_3 is estimated to be larger than 153 kcal/mol. This value is much larger than the available energy. Therefore, a dissociation mechanism occurring through isomerization to a linear molecule does not explain the presence of reaction (4). If 5-methyl-1-cyclopentene-3-yne is produced as an intermediate, followed by C-C bond cleavage, ΔH° for reaction (4) may still be as high as 126 kcal/mol, larger than the available energy at 248 nm. This means that, if 5-methyl-1-cyclopentene-3-yne dissociates to C_5H_3 and CH_3, the C_5H_3 structure must be more stable than 1-cyclopentene-3-ynal radical by at least 11 kcal/mol due to

the additional resonance energy of additional C-C bond formation. A structure similar to benzyne is a possibility. Therefore, dissociation through something resembling 5-methyl-1-cyclopentene-3-yne may be possible. In order to clarify the reaction mechanism for dissociation to C_5H_3 and CH_3, further study is needed.

V. CONCLUSIONS

When benzene in a molecular beam produced from a nozzle heated to 100-130°C was photolyzed under collision-free conditions at 193 and 248 nm, the following dissociation processes were observed. H, H_2 and CH_3 elimination (reactions (1), (2) and (4)) occurred after absorption of a single 193 nm photon, with relative yields from these primary channels of 0.8, 0.16, and 0.04 respectively. These reactions were found to occur from hot benzene produced following IC from S_2 to S_0. Some C_6H_5 produced by reaction (1) absorbed another photon and dissociated to C_4H_3 and C_2H_2 (reaction (6)). The H elimination reactions of C_6H_5 and C_6H_4 (reactions (3a) and (3b)) were also induced by absorption by C_6H_5 and C_6H_4, respectively. When benzene absorbed two photons, dissociation to two C_3H_3 occurred (reaction (8)).

When benzene was excited to S_1 at 248 nm, H_2 and CH_3 elimination occurred with relative yields of 0.96 and 0.04 for reactions (2) and (4), respectively. These reactions most likely occur from hot benzene. Some of the C_6H_4 produced by

reaction (2) absorbed another photon and dissociated to C_4H_2 and C_2H_2 (reaction (10)) and to C_6H_2 and H_2 (reaction (9)). Dissociation to two C_3H_3 occurred when benzene absorbed two photons.

ACKNOWLEDGMENT

We would like to thank Barbara Balko for technical assistance on the CMBA experiment and Pam Chu for bringing to our attention some references on the photochemistry of benzene. A. Y. also wishes to acknowledge financial support from the Science and Technology Agency of Japan. This work was supported by the Director, Office of Energy Research, Office of Basic Energy Sciences, Chemical Sciences Division of the U.S. Department of Energy under Contract No. DE-AC03-76SF00098.

REFERENCES

* Permanent address: Department of Chemistry, Japan Atomic Energy Research Institute, Tokai-mura, Naka-gun, Ibaraki 319-11, Japan.

1. C. S. Parmenter, Adv. Chem. Phys. **22**, 365 (1972).
2. L. D. Ziegler and B. S. Hudson, Excited States vol. 5, p.41 (Academic Press, New York, 1982).
3. J. K. Foote, M. H. Mallon, and J. N. Pitts, Jr., J. Am. Chem. Soc. **88**, 3698 (1966).
4. K. Shindo and S. Lipsky, J. Chem. Phys. **45**, 2292 (1966).
5. H. R. Ward, J. S. Wishnok, and P. D. Sherman, Jr., J. Am. Chem. Soc. **89**, 162 (1967).
6. L. Kaplan and K. E. Wilzbach, J. Am. Chem. Soc. **89**, 1030 (1967).
7. L. Kaplan, S. P. Walch, and K. E. Wilzbach, J. Am. Chem. Soc. **90**, 5646 (1968).
8. H. R. Ward and J. S. Wishnok, J. Am. Chem. Soc. **90**, 5353 (1968).
9. F. Mellows and S. Lipsky, J. Phys. Chem. **70**, 4076 (1966).
10. N. Nakashima and K. Yoshihara, J. Chem. Phys. **79**, 2727 (1983).
11. N. Nakashima and K. Yoshihara, J. Chem. Phys. **77**, 6040 (1982).
12. S. A. Lee, J. M. White, and W. A. Noyes, Jr., J. Chem. Phys. **65**, 2805 (1976).

13. L. Kaplan and K. E. Wilzbach, J. Am. Chem. Soc. **90**, 3291 (1968).

14. J. P. Reilly and K. L. Kompa, J. Chem. Phys. **73**, 5468 (1980).

15. V. S. Letokhov, **Laser Photoionization Spectroscopy** (Academic Press, Orlando, 1987).

16. X. Zhao, E. J. Hintsa, and Y. T. Lee, J. Chem. Phys. **88**, 801 (1988).

17. X. Zhao, W. B. Miller, E. J. Hintsa, and Y. T. Lee, J. Chem. Phys., in press.

18. X. Zhao, R. E. Continetti, A. Yokoyama, E. J. Hintsa, and Y. T. Lee, J. Chem. Phys., submitted.

19. A. M. Wodtke and Y. T. Lee, J. Phys. Chem. **89**, 4744 (1985).

20. R. E. Continetti, B. A. Balko, and Y. T. Lee, in preparation.

21. A. M. Wodtke, E. J. Hintsa, J. Somorjai, and Y. T. Lee, J. Israeli Chem., submitted; E. J. Hintsa, private communication.

22. V. S. Rao and G. B. Skinner, J. Phys. Chem. **92**, 2442 (1988) and references therein.

23. E. J. Hintsa, A. M. Wodtke, and Y. T. Lee, J. Phys. Chem. **92**, 5379 (1988).

24. S. W. Benson, **Thermochemical Kinetics** (Wiley, New York, 1977).

25. W. Hack and W. Langel, Il Nuovo Cimento **63B**, 207 (1981).

26. N. Nakashima, H. Inoue, M. Sumitani, and K. Yoshihara, J. Chem. Phys. **73**, 5976 (1980).

27. W. Dietz, H. J. Neusser, U. Boesl, and E. W. Schlag, Chem. Phys. **66**, 105 (1982).

28. J. R. Reeher, G. D. Flesch, and H. J. Svec, Org. Mass Spectrom. **11**, 154 (1976); J. R. Reeher, G. D. Flesch, and H. J. Svec, Int. J. Mass Spectrom. Ion Phys. **19**, 351 (1976).

29. S. K. Pollack and W. J. Hehre, Tetrahedron Lett. **21**, 2483 (1980).

30. H. E. O'Neal and S. W. Benson, in **Free Radicals**, J. Kochi, ed. (Wiley, New York, 1973).

31. J. H. Kiefer, L. J. Mizerka, M. R. Patel, and H.-C. Wei, J. Phys. Chem. **89**, 2013 (1985).

32. J. L. Franklin, J. G. Dillard, H. M. Rosenstock, J. T. Herron, K. Draxl, and F. H. Field, NSRDS-NBS **26** (U.S. Dept. of Commerce, Washington, DC, 1969).

Table 1. Signal intensity of the fast component in the m/e = 48-52 TOF spectra in units of counts/pulse at 15° at 193 and 12.3° at 248 nm.

m/e	193 nm[a)]	248 nm[b)]
52	N.S.[c)]	N.S.
51	0.370	0.023
50	0.533	0.273
49	0.614	0.240
48	0.248	0.075

a) Normalized at a laser intensity of 5 MW/cm^2
b) Normalized at a laser intensity of 30 MW/cm^2.
c) N.S. = No signal

Table 2. Reaction channels, average and maximum translational energy release, and heats of reaction at 298 K.[a]

	Reaction	λ(nm)	$\langle E_T \rangle$	$E_{T,max}$	$h\nu - E_{T,max}$	$\Delta H°$[b]
(1)	$C_6H_6 \rightarrow C_6H_5 + H$	193	4.98	39	109	110.8±1
(2)	$C_6H_6 \rightarrow C_6H_4 + H_2$	193	16.03	47.5	100.5	98.2±5
		248	7.68	22.5	92.5	
(4)	$C_6H_6 \rightarrow C_5H_3 + CH_3$	193	13.14	34	114	
		248	8.25	30	85	
(8)	$C_6H_6 \rightarrow 2C_3H_3$	193	13.89	52	244[c]	152.4±2
		248	8.37	38	192[c]	
(3a)	$C_6H_5 \rightarrow C_6H_4 + H$	193	4.98	39	218[d]	91.6±6
(6)	$C_6H_5 \rightarrow C_4H_3 + C_2H_2$	193	17.22	58	199[e]	101.7
(3b)	$C_6H_4 \rightarrow C_6H_3 + H$	193	4.98	39	209.5[f]	
(9)	$C_6H_4 \rightarrow C_6H_2 + H_2$	248	24.72	40.5	167[g]	
(10)	$C_6H_4 \rightarrow C_4H_2 + C_2H_2$	248	18.81	62.5	145[h]	38.2

---

a) All energies in kcal/mol.

b) Calculated from the heats of formation of benzene (19.8), phenyl radical (78.5±1), H (52.1), and C_2H_2 (54.2) from ref. 24; benzyne (118±5) from ref. 29; $CH_2{\equiv}C{-}CH$ (86.1) from ref. 30; $CH{=}CH{-}C{\equiv}CH$ (126) from ref. 31; and $CH{\equiv}C{-}C{\equiv}CH$ (102) from ref. 32.

c) $2h\nu - E_{T,max}$.

d) $2h\nu - E_{T,max}(C_6H_6 \rightarrow C_6H_5 + H) - E_{T,max}(C_6H_5 \rightarrow C_6H_4 + H)$.

e) $2h\nu - E_{T,max}(C_6H_6 \rightarrow C_6H_5 + H) - E_{T,max}(C_6H_5 \rightarrow C_4H_3 + C_2H_2)$.

f) $2h\nu - E_{T,max}(C_6H_6 \rightarrow C_6H_4 + H_2) - E_{T,max}(C_6H_4 \rightarrow C_6H_3 + H)$.

g) $2h\nu - E_{T,max}(C_6H_6 \rightarrow C_6H_4 + H_2) - E_{T,max}(C_6H_4 \rightarrow C_6H_2 + H_2)$.

h) $2h\nu - E_{T,max}(C_6H_6 \rightarrow C_6H_4 + H_2) - E_{T,max}(C_6H_4 \rightarrow C_4H_2 + C_2H_2)$.

Table 3. Estimated heats of formation of benzene isomers.[a)]

molecule	heat of formation (kcal/mol)
1,3-Hexadiyne	98
1,4-Hexadiyne	95
2,4-Hexadiyne	93
5-methyl-1-Cyclopentene-3-yne	66

a) Calculated as described in ref. 24.

FIGURE CAPTIONS

Fig. 1 TOF spectra at 193 nm. Open circles represent the data throughout.

(a) m/e = 77: ———; calculated spectrum using the $P(E_T)$ for reaction (1) shown in Fig. 2.

(b) m/e = 1: – – –; contribution of H atoms from reaction (1), — · —; H atoms from secondary reaction (3a).

Fig. 2 Center-of-mass translational energy distribution for reaction (1) (H atom elimination) at 193 nm.

Fig. 3 (a) m/e = 76 TOF spectrum at 193 nm.

————; total calculated signal, – – – –; C_6H_5 from reaction (1), — · —; C_6H_4 from reaction (2).

(b) Laser power dependence of the m/e = 75 TOF spectrum at 193nm. ○ ; 8.4 mJ/pulse, ● ; 0.34 mJ/pulse.

Fig. 4 $P(E_T)$ for reaction (2) (H_2 elimination) at (a) 193 nm and (b) 248 nm.

Fig. 5 (a) m/e = 62 TOF spectrum at 193 nm.

– – – –; C_6H_5 from reaction (1), — · —; C_6H_4 from reaction (2), —— ——; of C_5H_3 from reaction (4).

(b) m/e = 18 TOF spectrum, from the dissociation of C_6D_6 at 193 nm. ——; calculated using the $P(E_T)$ for reaction (4) shown in Fig. 6(a).

Fig. 6 $P(E_T)$ for reaction (4) (CH_3 elimination) at (a) 193 nm and (b) 248 nm.

Fig. 7 (a) m/e = 51 TOF spectrum at 193 nm.
– – – –; C_6H_5 from reaction (1), — · —; C_6H_4 from reaction (2), — —; C_6H_4 from reaction (3a), ·····; C_6H_3 from reaction (3b), — – —; C_4H_3 from reaction (6).
(b) m/e = 26 TOF spectrum at 193 nm.
Slow peak; C_6H_4 from reaction (2), fast peak; C_2H_2 from reaction (6), with small contributions from reactions (1) not shown, and (4).

Fig. 8 $P(E_T)$'s for (a) reaction (6) at 193 nm and (b) reaction (10) at 248 nm.

Fig. 9 m/e = 39 TOF spectrum at 193 nm.
— · — (slow); C_6H_4 from reaction (2), — —; C_5H_3 from reaction (4), ·····; C_4H_3 from reaction (6), — – — (fast); C_3H_3 from reaction (8).

Fig. 10 $P(E_T)$ for reaction (8) at (a) 193 nm and (b) 248 nm.

Fig. 11 (a) m/e = 76 TOF spectrum at 248 nm.
——; fit with the $P(E_T)$ for reaction (2) shown in Fig. 4(b).
(b) Laser power dependence of the m/e = 73 TOF spectrum at 248 nm. ○ ; 68 mJ/pulse, ● ; 11 mJ/pulse.

Fig. 12 $P(E_T)$ for reaction (9) at 248 nm.

Fig. 13 m/e = 61 TOF spectrum at 248 nm.
– – – –; C_6H_4 from reaction (2), — · —; C_5H_3 from reaction (4).

Fig. 14 m/e = 50 TOF spectrum at 248 nm.

Slow peak; C_6H_4 from reaction (2), middle; C_5H_3 from reaction (4), fast peak; C_4H_2 from reaction (10).

Fig. 15 m/e = 39 TOF spectrum at 248 nm.

– – – –; C_6H_4 from reaction (2), — · —; C_5H_3 from reaction (4), —— ——; C_3H_3 from reaction (8).

Fig. 16 Excitation scheme for excitation at 193 nm. σ's are the respective cross-sections, τ is the lifetime of S_2, and k is the dissociation rate constant from S_0^*. See text.

Fig. 17 Power dependences of the fragment yields of benzene at 193 nm.

(a) C_5H_3 observed at m/e = 62. Curves show the calculated power dependence for the one photon process. – – – –; $k = 1 \times 10^8\ s^{-1}$, ———; $k = 5 \times 10^7\ s^{-1}$, — · —; $k = 3 \times 10^5\ s^{-1}$.

(b) C_3H_3 observed at m/e = 39 (●) and m/e = 37 (○). Curves show the calculated power dependence for the two photon process with $k = 5 \times 10^7\ s^{-1}$.

(c) C_4H_3 and C_2H_2 observed at m/e = 48 (●) and m/e = 25 (○), respectively. – – – –; calculated power dependence for the two photon process with $k = 5 \times 10^7\ s^{-1}$. ———; best fit curve for the secondary photodissociation process with $k = 5 \times 10^7\ s^{-1}$.

(d) C_6H_5 (●) from reaction (1) and C_6H_4 (○) from reaction (3a) observed at m/e = 75. ———; calculated

power dependence for the one photon process with k = 5×10^7 s^{-1}. – – – –; calculated power dependence for secondary photodissociation with k = 5×10^7 s^{-1}. (e) C_6H_4 (●) from reaction (2) and C_6H_3 (○) from reaction (3b) observed at m/e = 75. ——; calculated power dependence for the one photon process with k = 5×10^7 s^{-1}. – – – –; calculated power dependence for secondary photodissociation with k = 5×10^7 s^{-1}.

Fig. 18 Power dependences of fragment yields from the photodissociation of benzene at 248 nm.

(a) C_5H_3 observed at m/e = 61. Curve shows the calculated power dependence for the one photon process.

(b) C_3H_3 observed at m/e = 37. Curve shows the calculated power dependence for the two photon process.

(c) C_4H_2 observed at m/e = 49. Curve shows the calculated power dependence for secondary photodissociation with $\sigma_4 = 1 \times 10^{-17}$ cm^2.

(d) C_6H_4 (●) from reaction (2) and C_6H_3 (○) from reaction (9) observed at m/e = 73. ——; calculated power dependence for the one photon process with $\sigma_4 = 1 \times 10^{-17}$ cm^2. – – – –; calculated power dependence for secondary photodissociation with $\sigma_4 = 1 \times 10^{-17}$ cm^2.

Fig. 19 Schematic view of dissociation mechanism observed for C_6H_6 dissociation at 193 nm. ‡ vibrationally exerted species, * electronically excited species, + ionic species.

Fig. 20 Schematic view of dissociation mechanism observed for C_6H_6 dissociation at 248 nm.

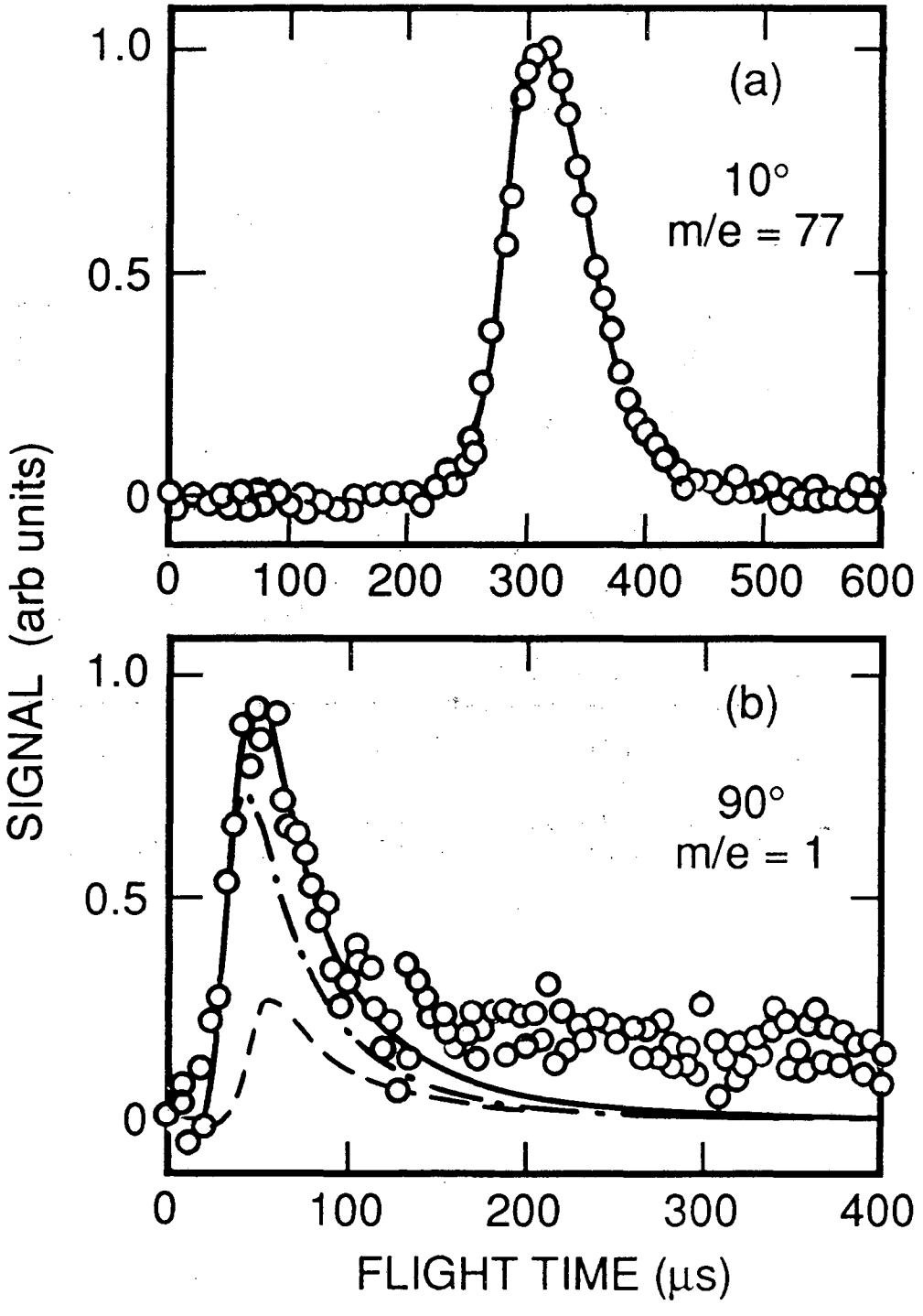

XBL 898-3096

Fig. 1

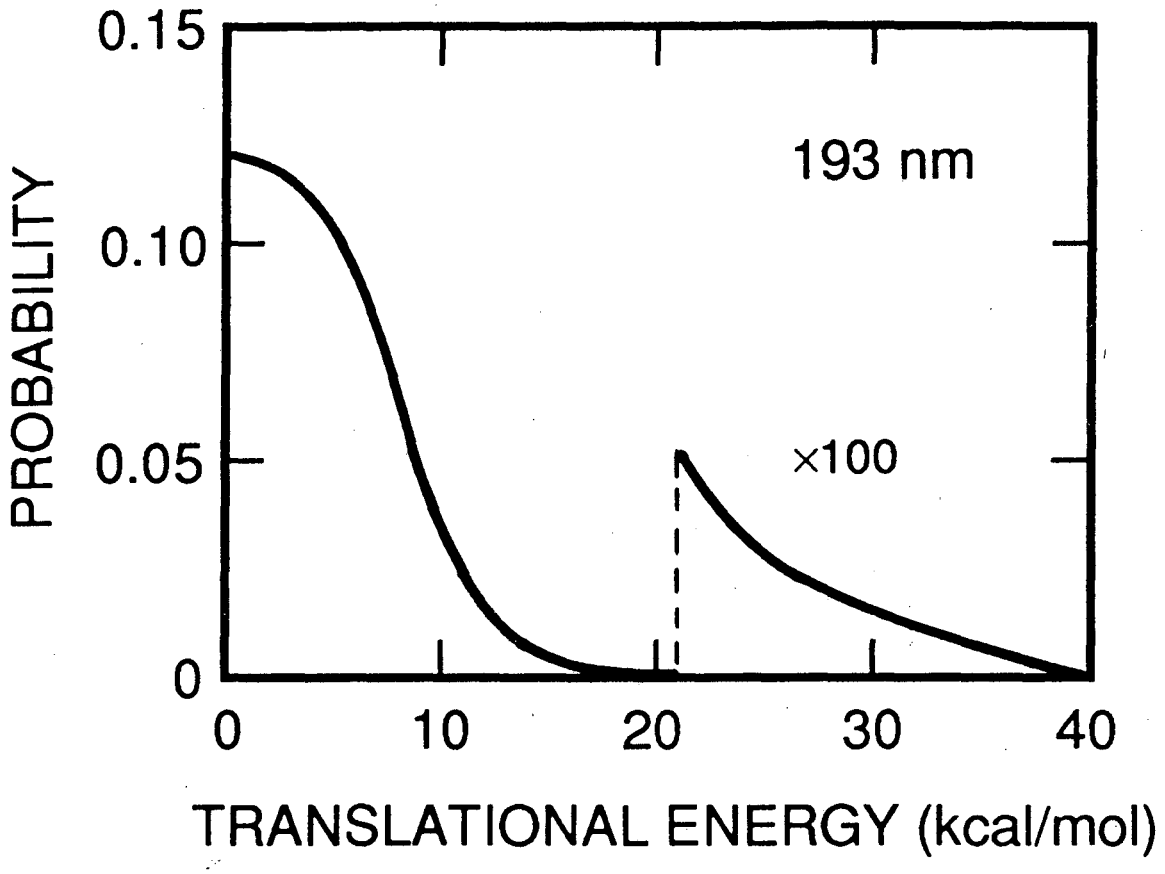

XBL 897-2801

Fig. 2

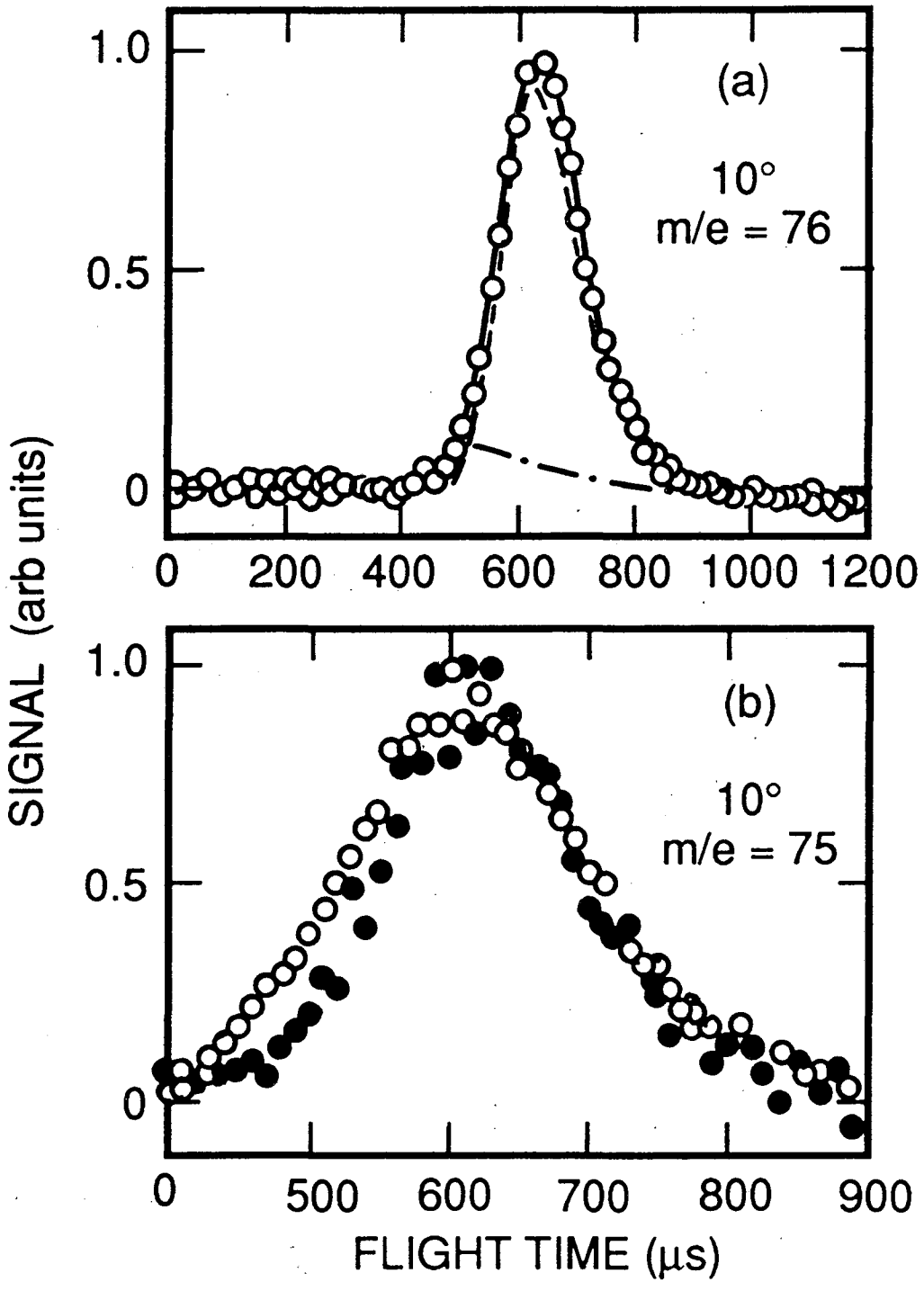

XBL 898-3097

Fig. 3

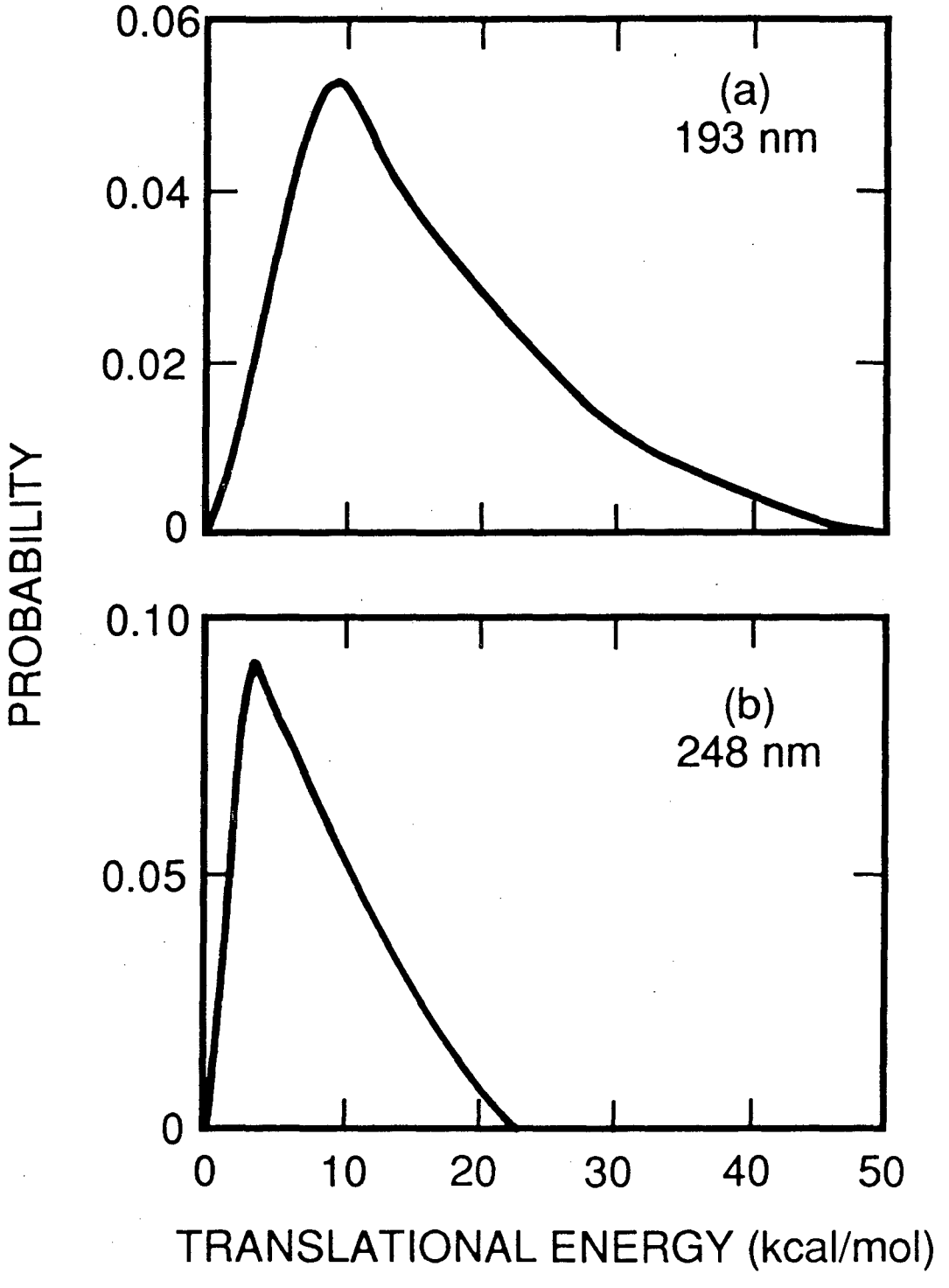

XBL 897-2802

Fig. 4

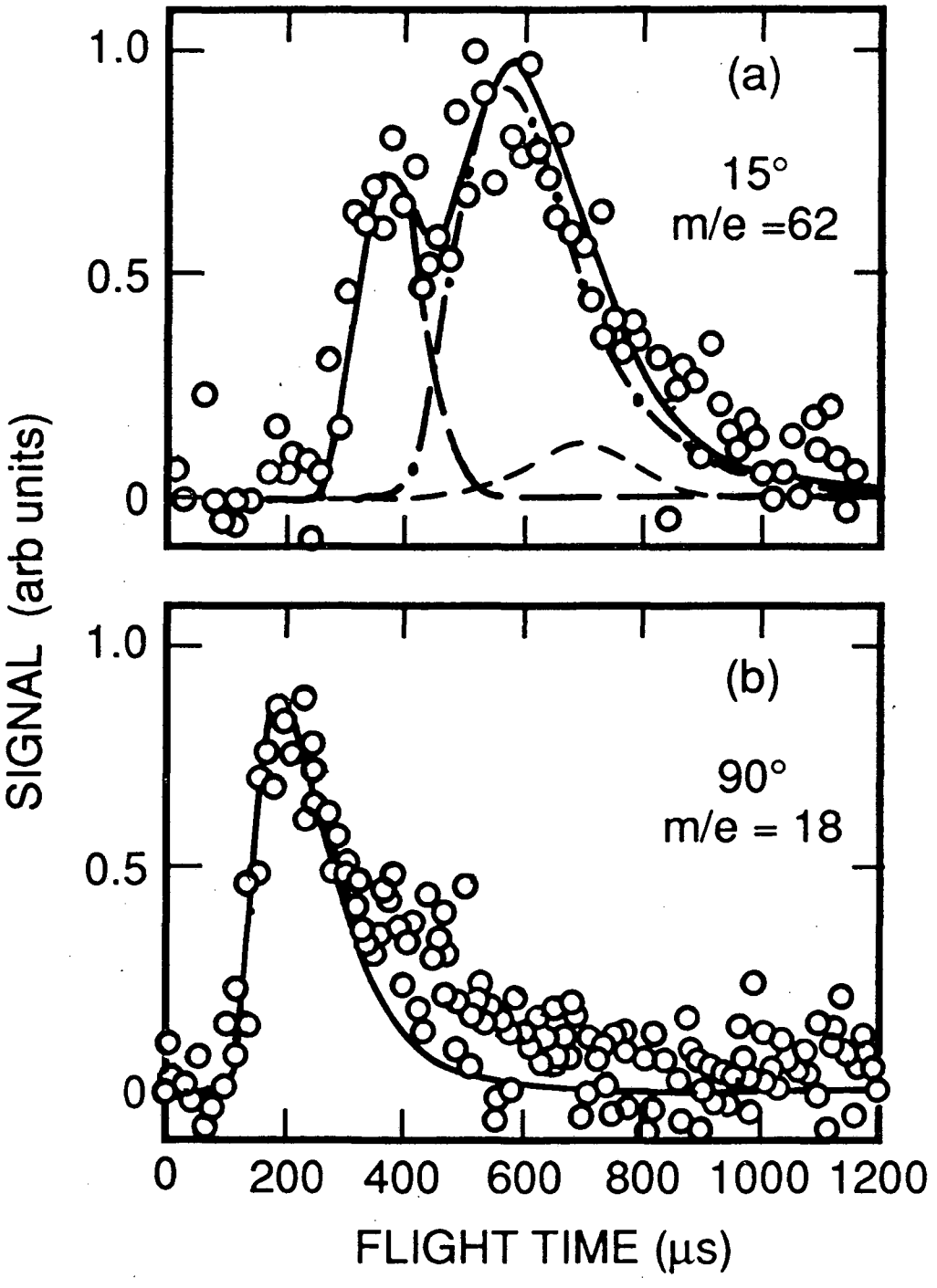

XBL 898-3098

Fig. 5

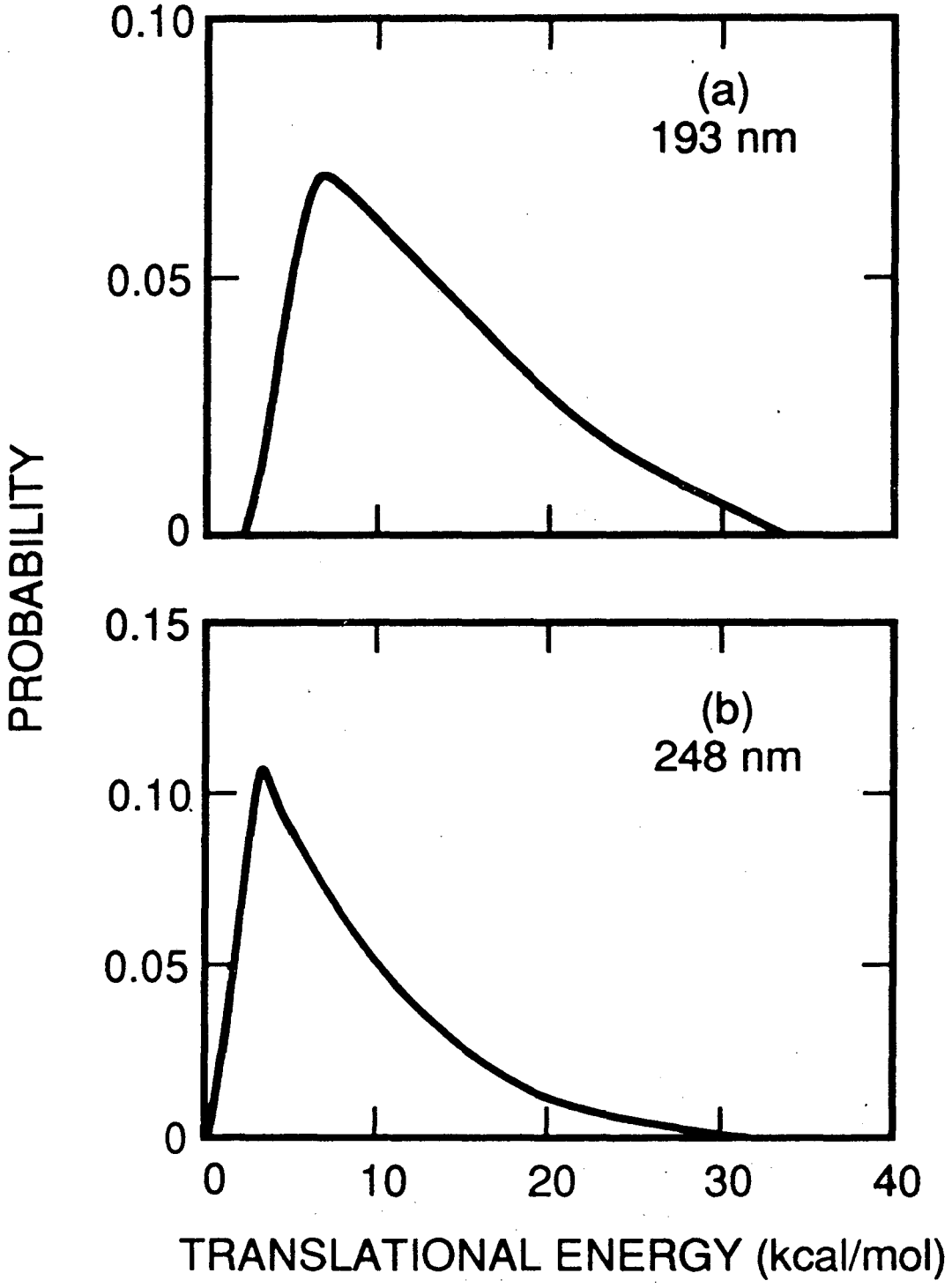

XBL 897-2803

Fig. 6

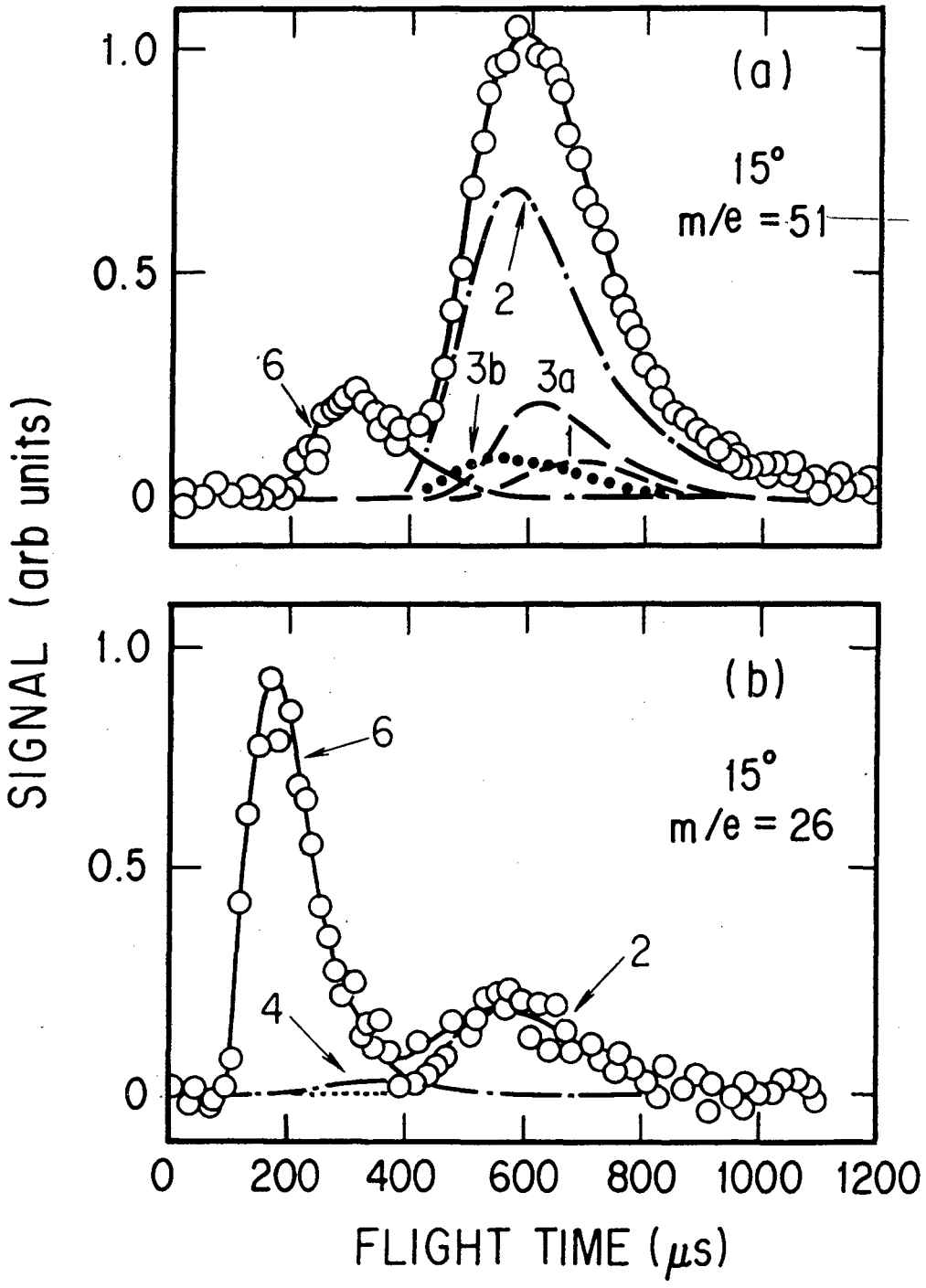

XBL 899-3504

Fig. 7

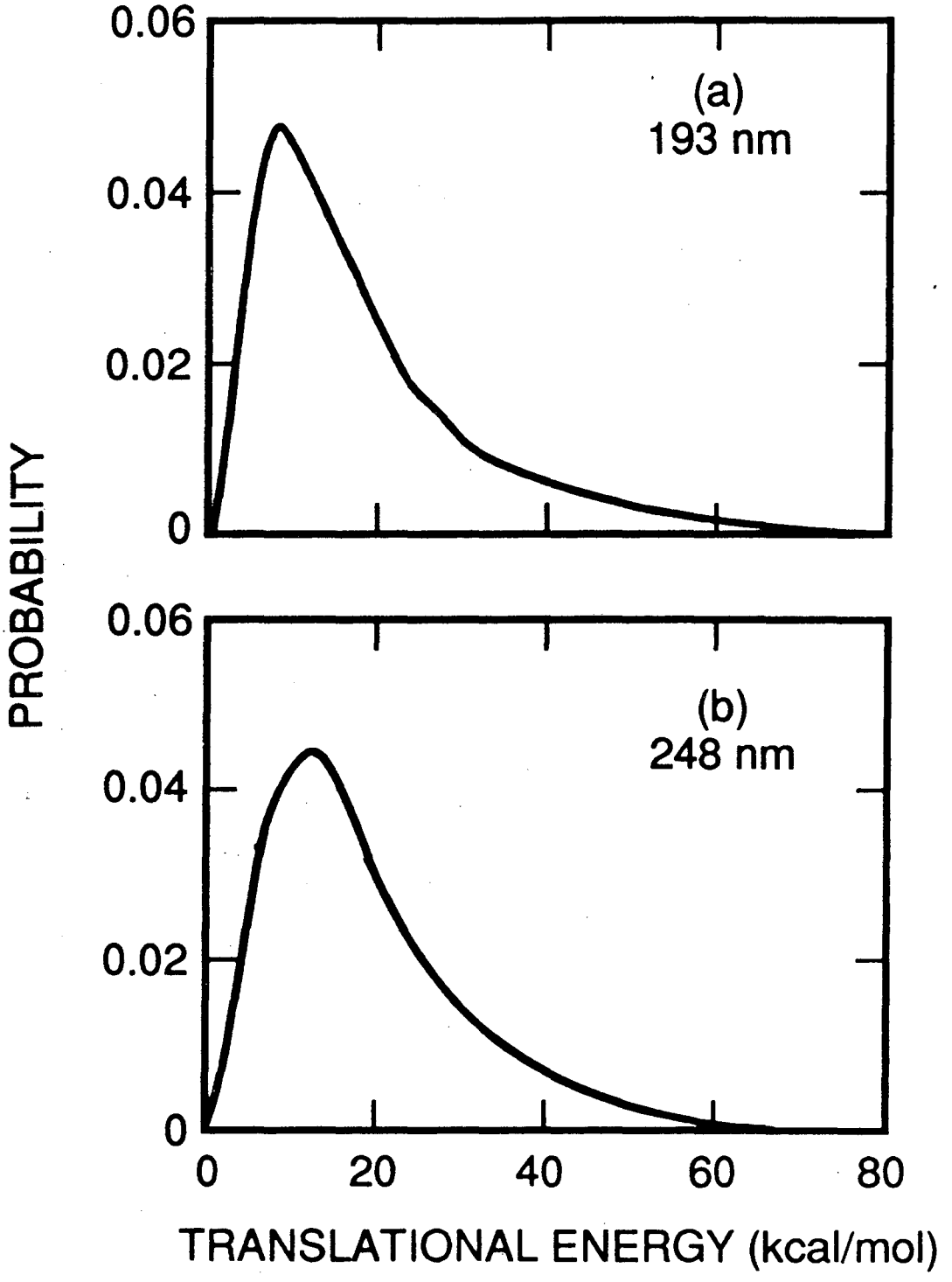

XBL 897-2804

Fig. 8

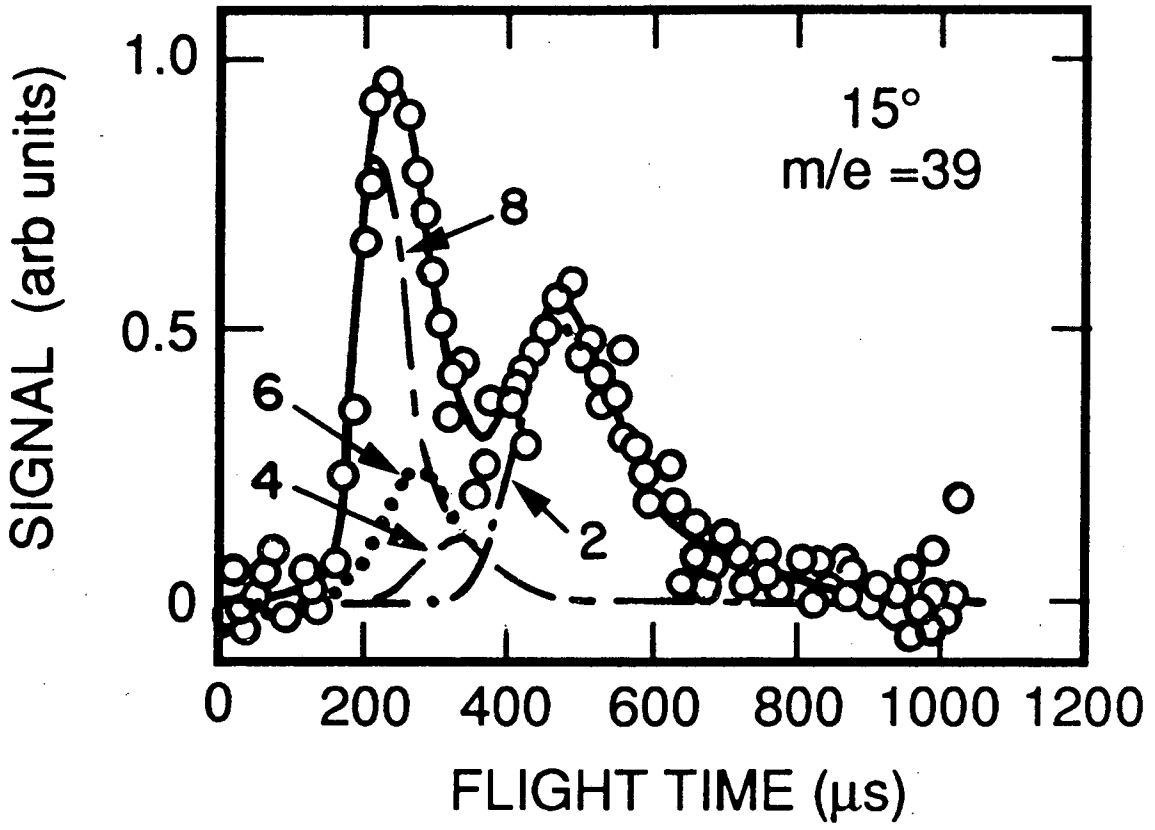
SIGNAL (arb units)
1.0
0.5
0
15°
m/e =39
8
6
4
2
0
200
400
600
800
1000
1200
FLIGHT TIME (μs)
XBL 898-3100

Fig. 9

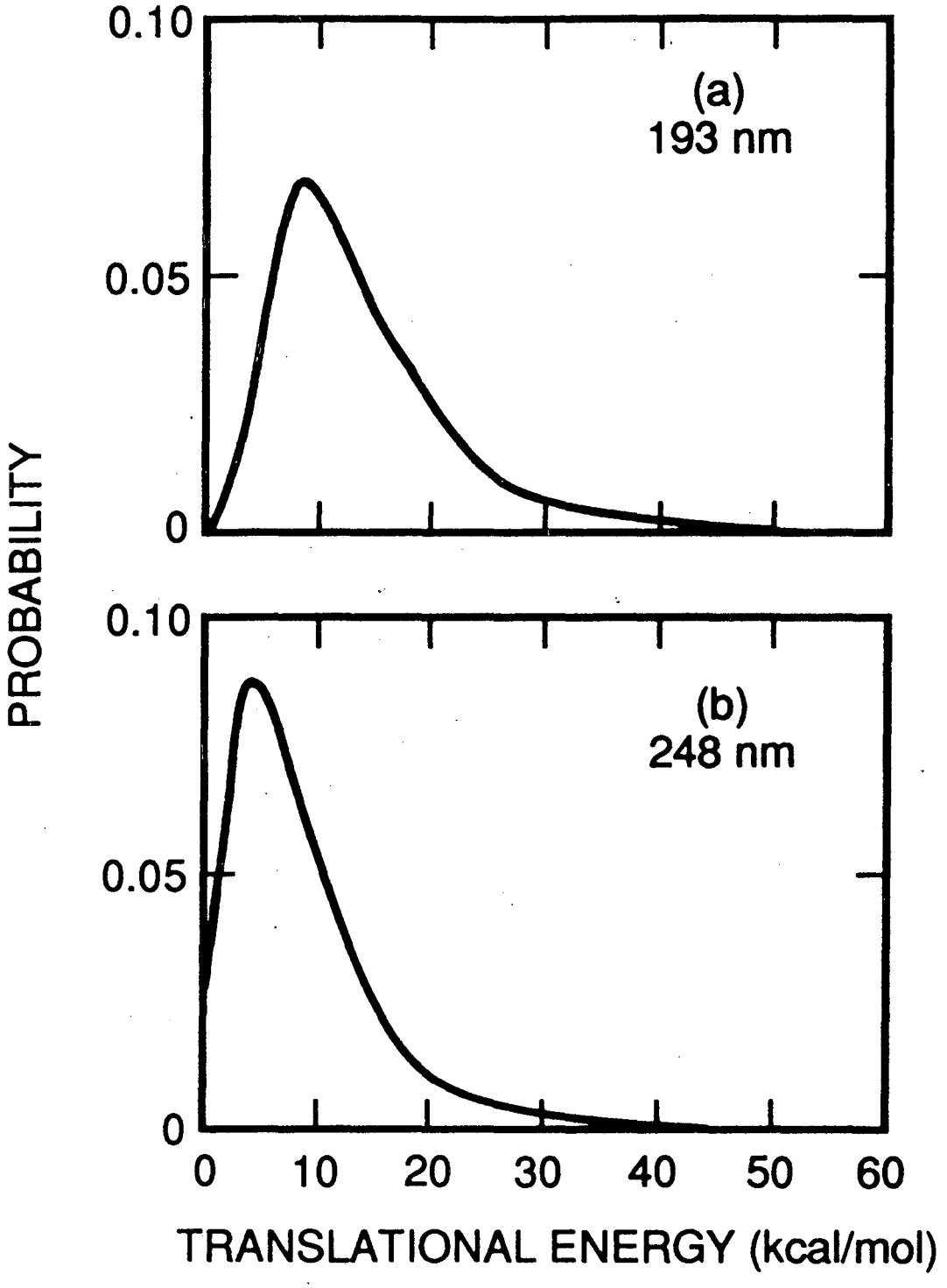

XBL 897-2805

Fig. 10

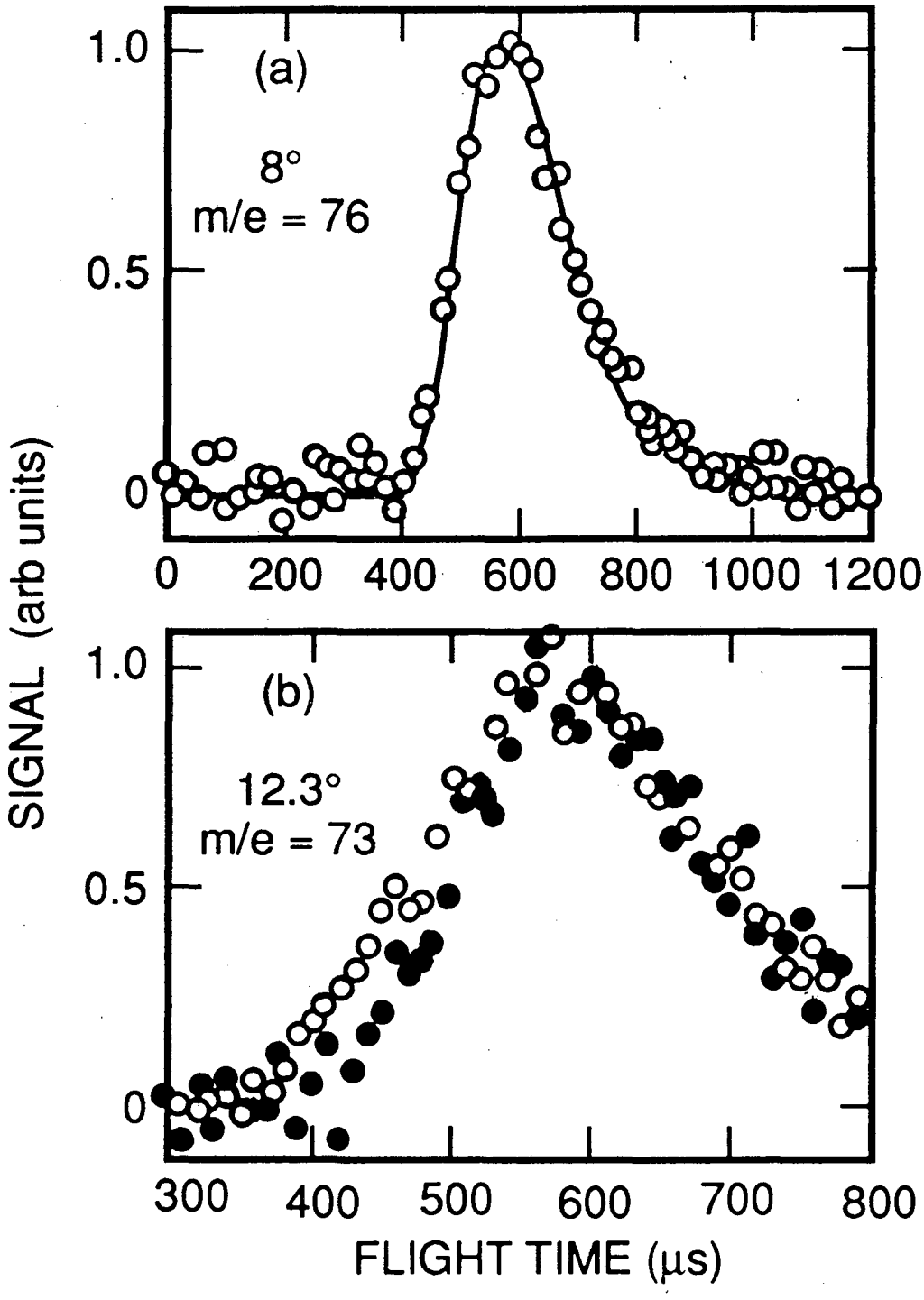

XBL 898-3101

Fig. 11

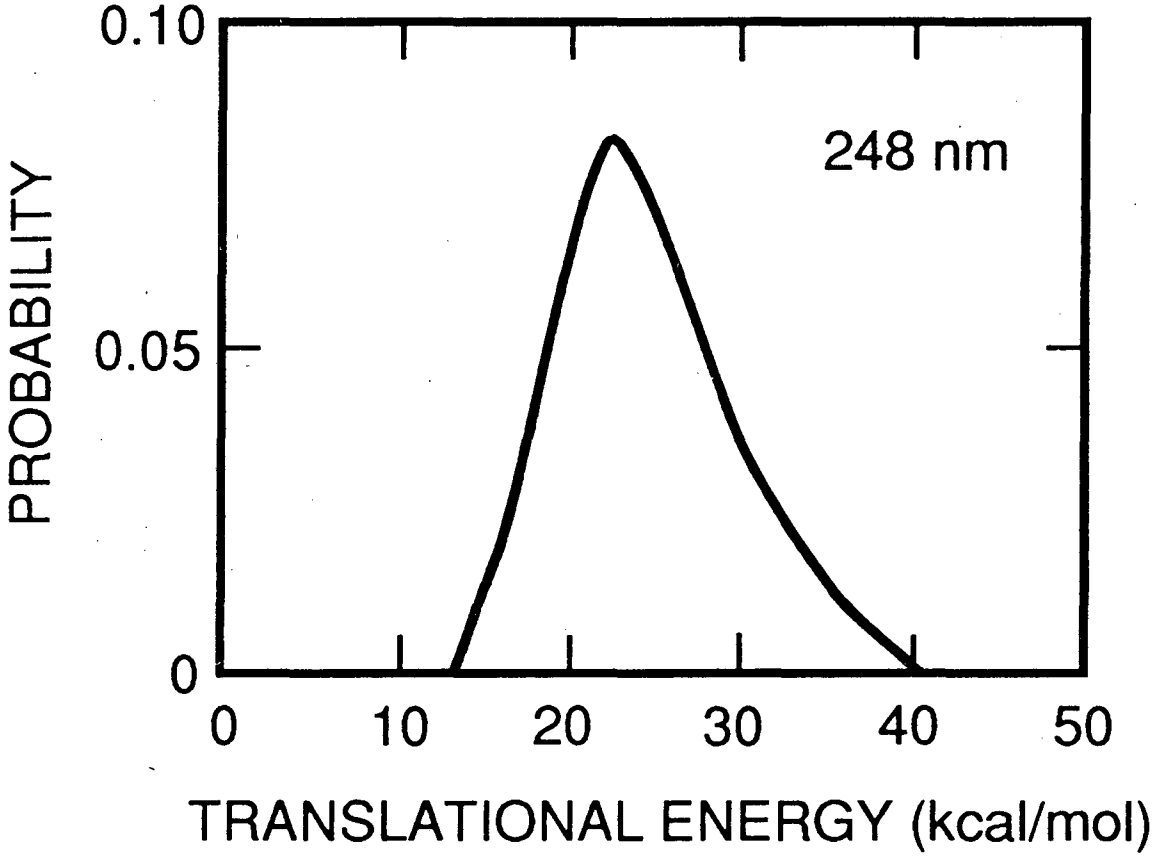

XBL 897-2806

Fig. 12

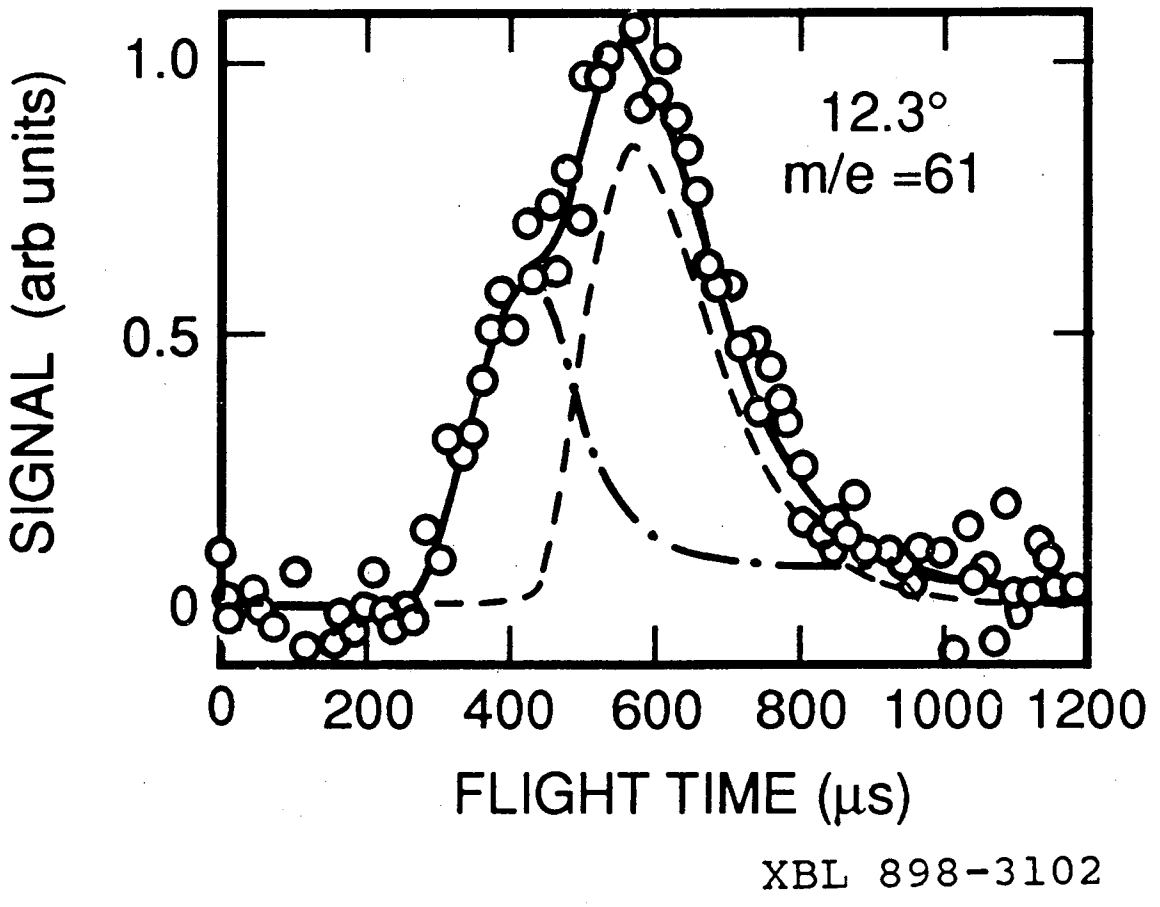
SIGNAL (arb units)
1.0
0.5
0
12.3°
m/e =61
b
0
200
400
600
800
1000
1200
FLIGHT TIME (μs)
XBL 898-3102

Fig. 13

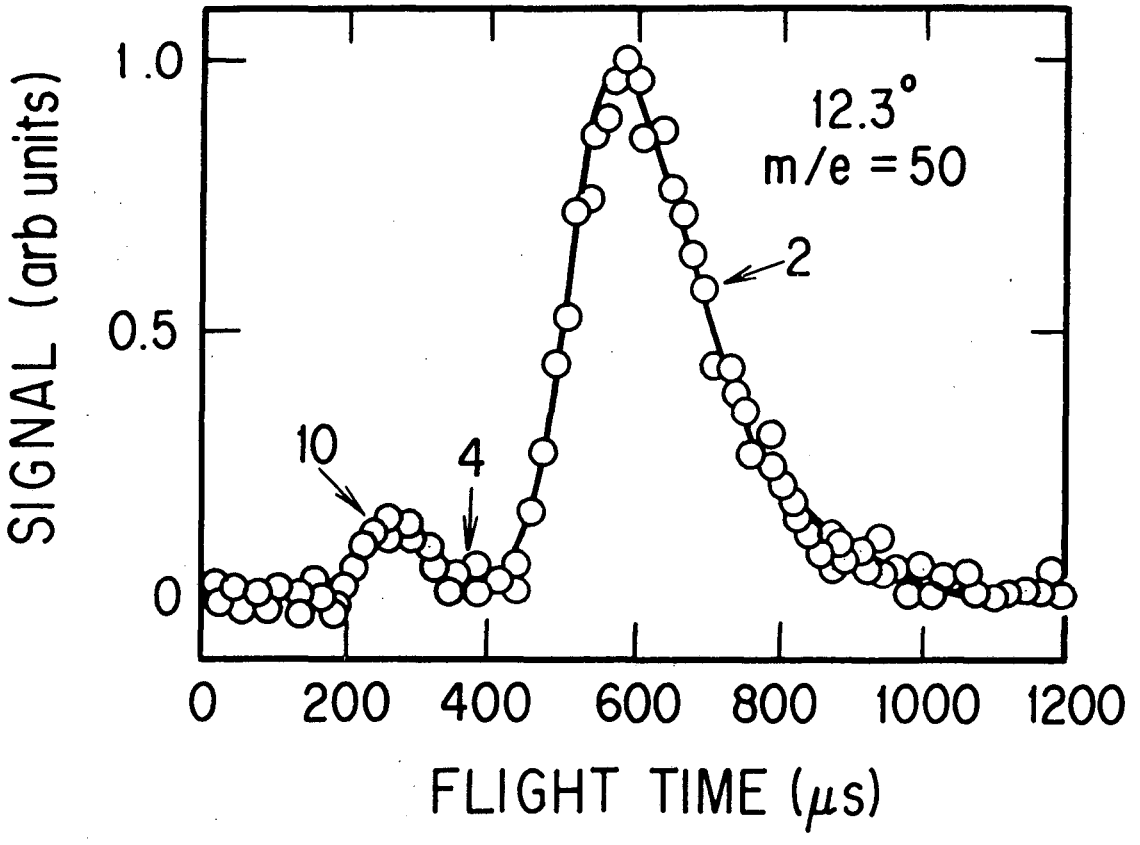

XBL 899-3503

Fig. 14

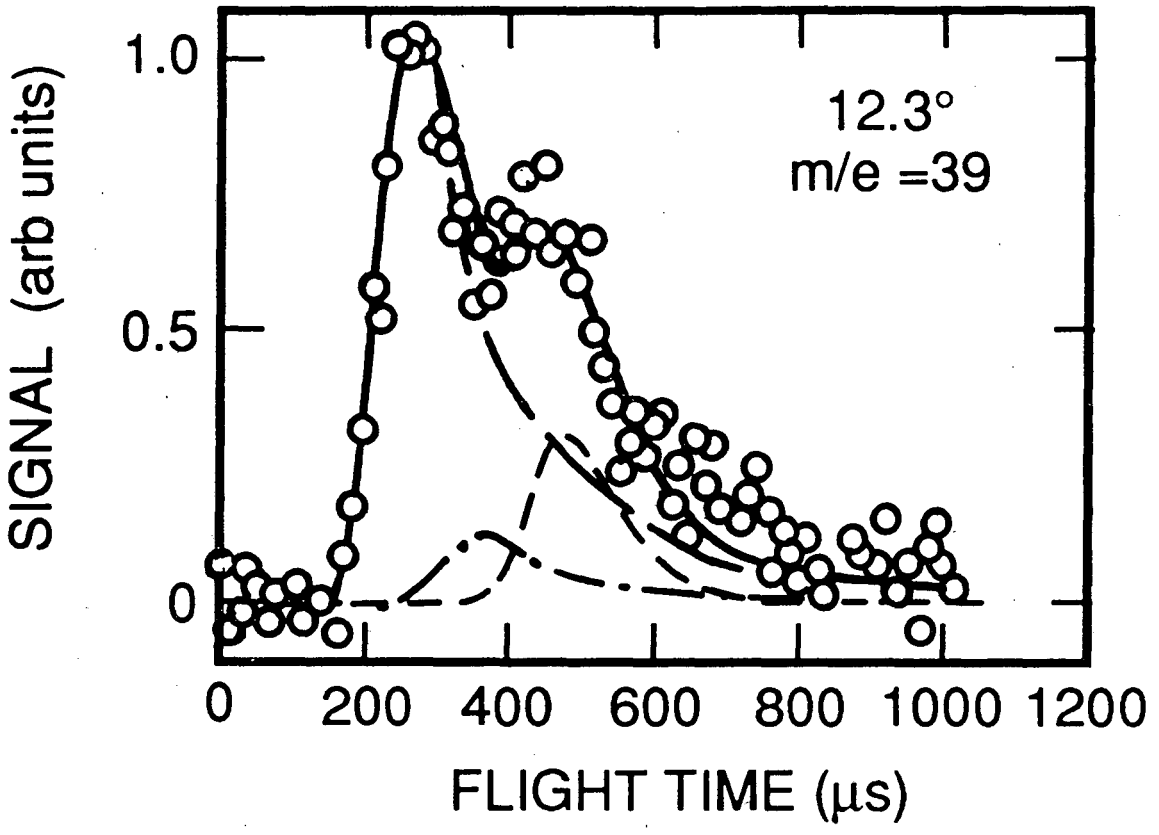

XBL 898-3104

Fig. 15

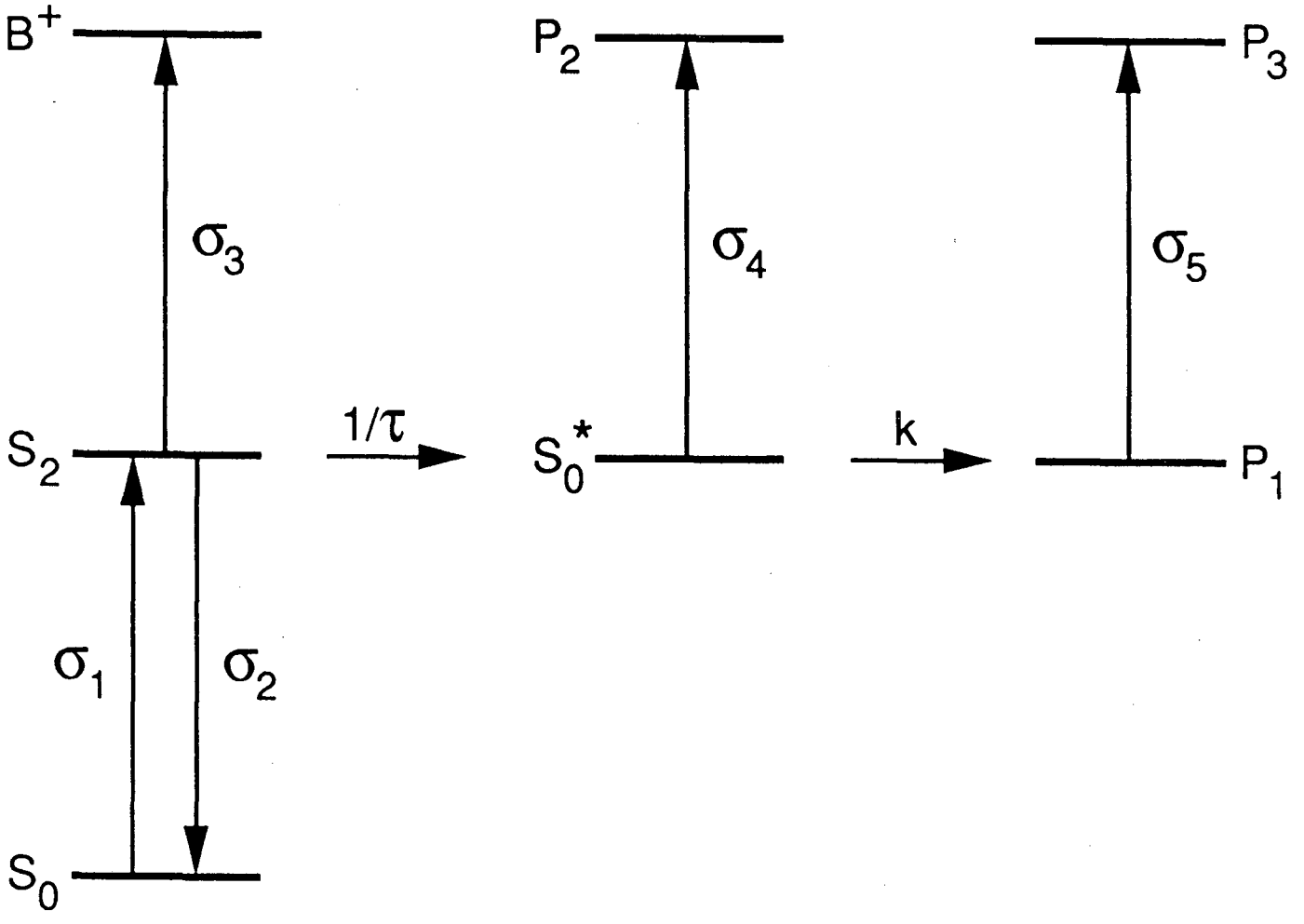

XBL 898-3105

Fig. 16

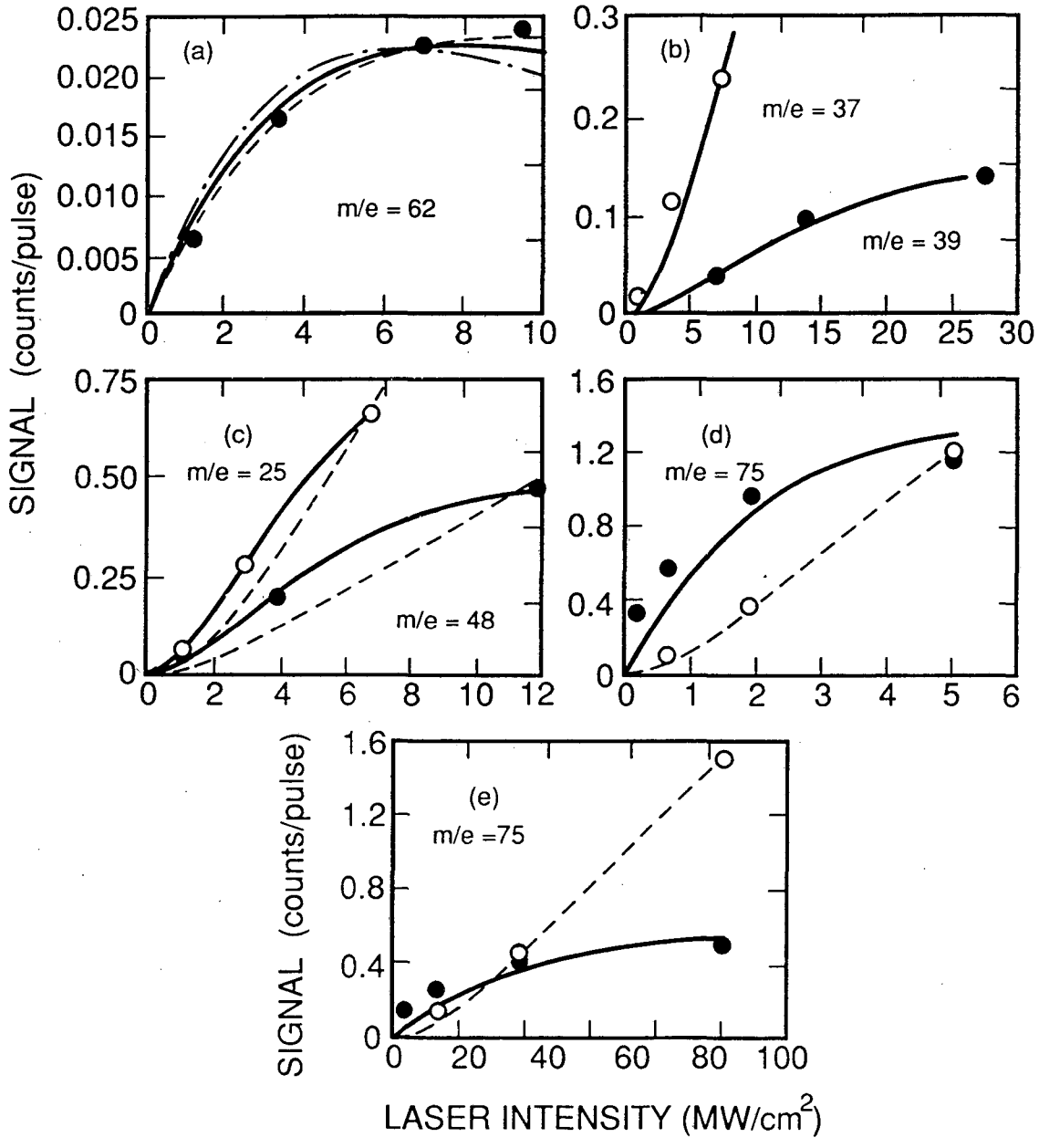

XBL 898-3106

Fig. 17

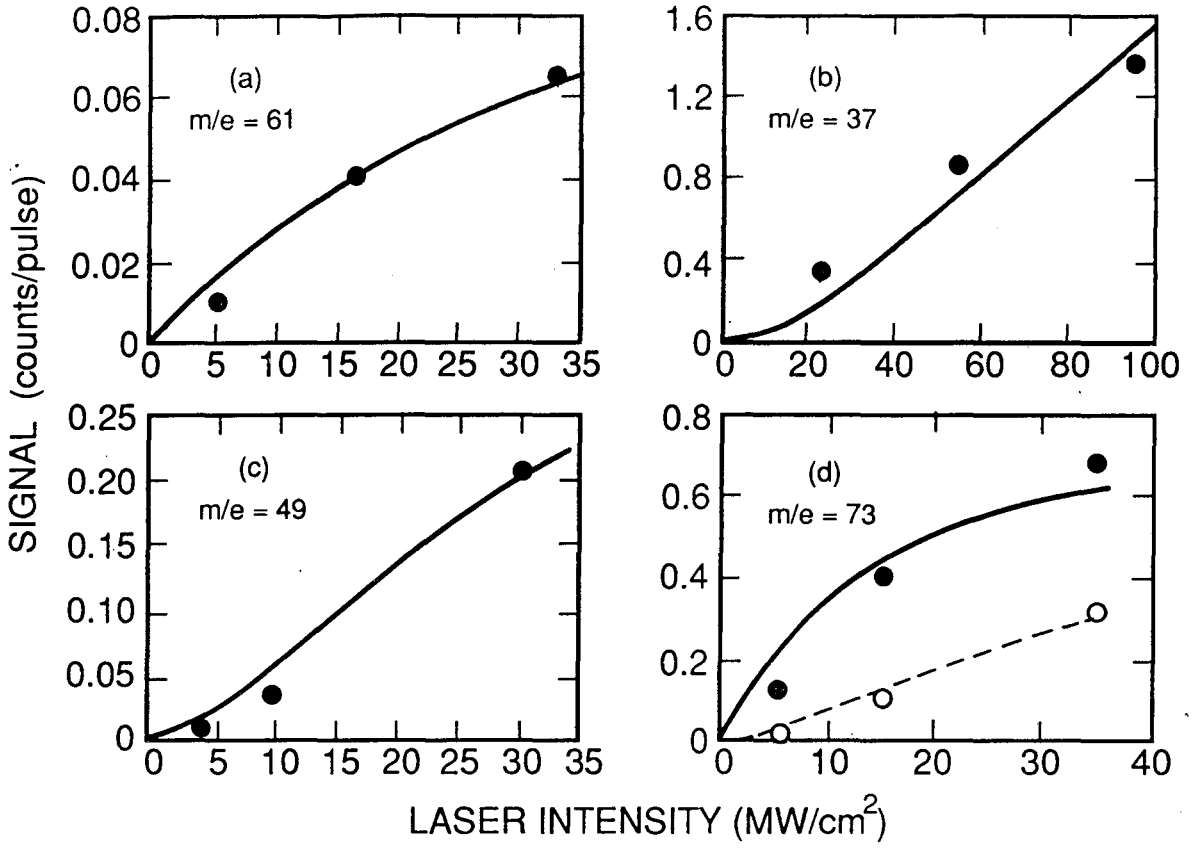

XBL 898-3107

Fig. 18

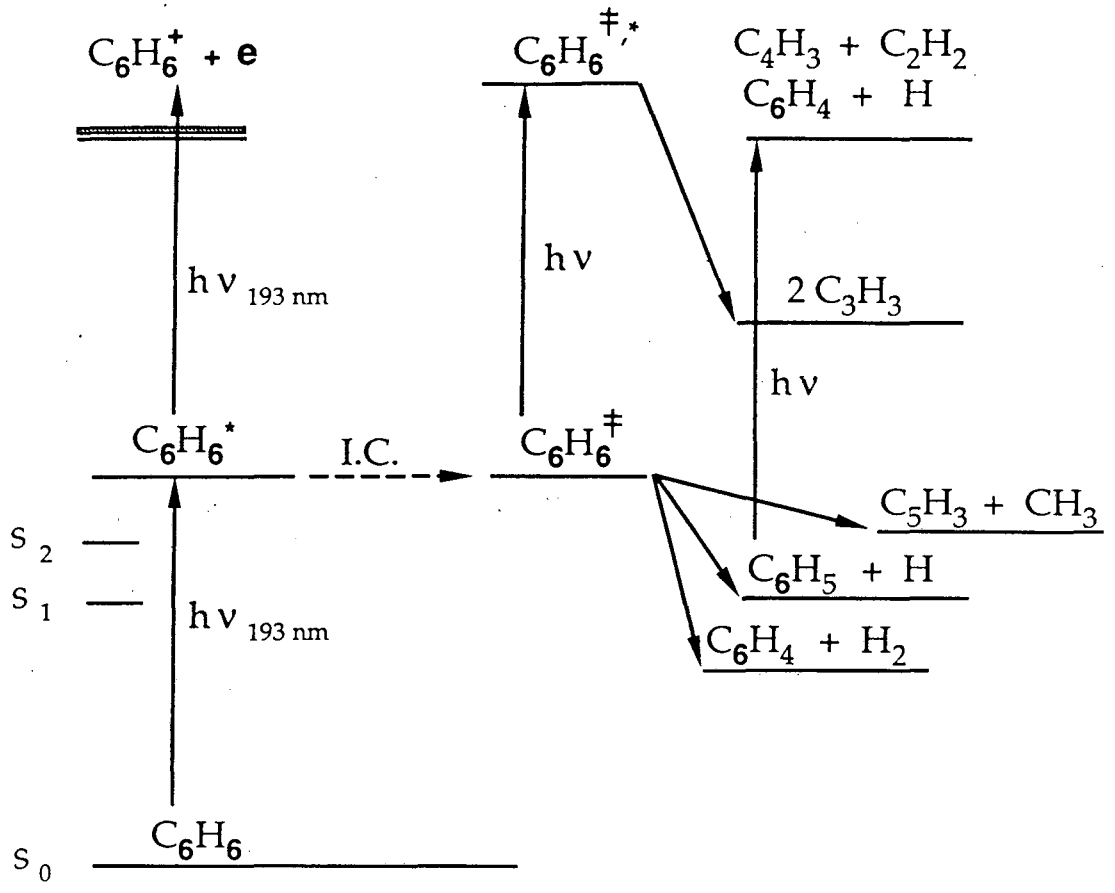

XBL 897-2800

Fig. 19

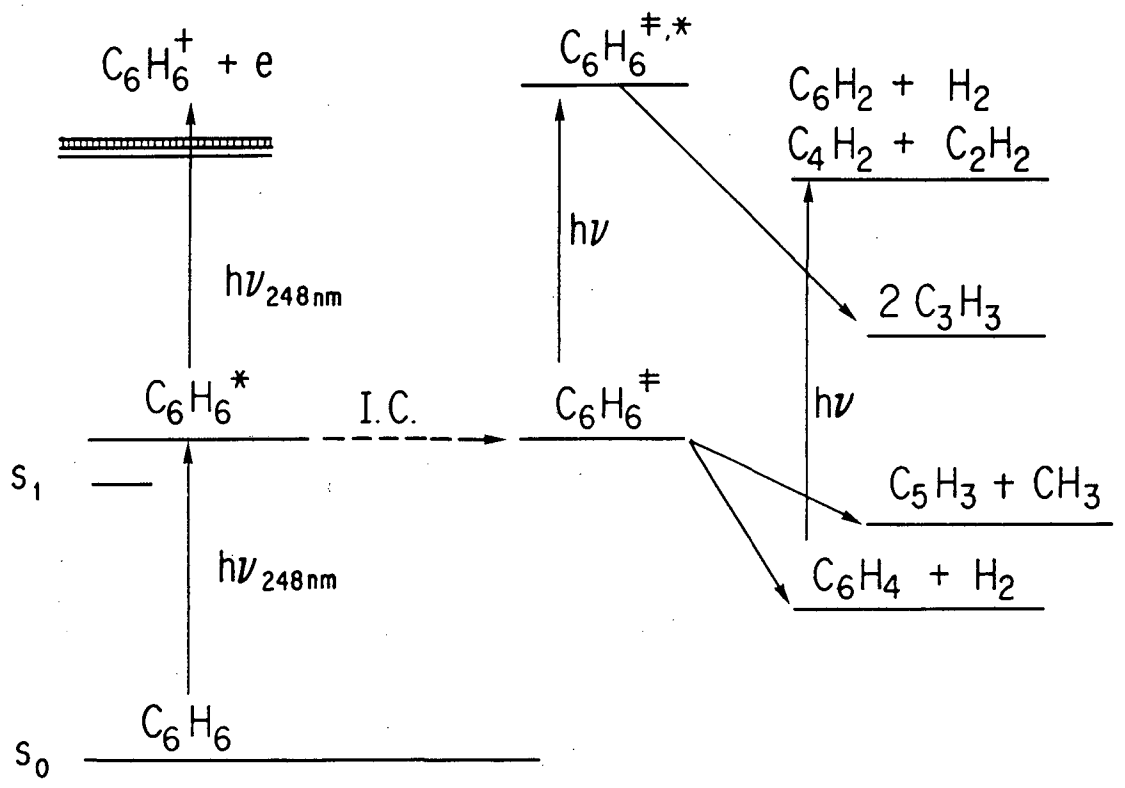

XBL 897-2799A

Fig. 20

LAWRENCE BERKELEY LABORATORY
TECHNICAL INFORMATION DEPARTMENT
1 CYCLOTRON ROAD
BERKELEY, CALIFORNIA 94720